Ozone pollution during the COVID-19 lockdown in the spring 2020 over Europe analysed from satellite observations, in situ measurements and models

5   Juan Cuesta[1], Lorenzo Costantino[2], Matthias Beekmann[3], Guillaume Siour[1], Laurent Menut[4], Bertrand Bessagnet[4,5], Tony C. Landi[6], Gaëlle Dufour[3] and Maxim Eremenko[1]

[1] Univ Paris Est Creteil and Université de Paris, CNRS, LISA, F-94010 Créteil, France

[2] Centre For Research On Energy And Clean Air (CREA), Hiihtomaentie 38 B 24 00800 Helsinki, Finland

10 [3] Université de Paris and Univ Paris Est Creteil, CNRS, LISA, F-75013 Paris, France

[4] Laboratoire de Météorologie Dynamique (LMD), Ecole Polytechnique, IPSL Research University, Ecole Normale Supérieure, Université Paris-Saclay, Sorbonne Universités, UPMC Univ Paris 06, CNRS, Route de Saclay, 91128 Palaiseau, France.

[5] Now at European Commision, Joint Research Centre, Via Fermi 2749, Ispra, Italy

15 [6] Via Fermi 2749, Ispra, ItalyNational Research Council, Institute of Atmospheric Sciences and Climate (ISAC-CNR), via Gobetti 101, 40129, Bologna, Italy

Correspondence to: Juan Cuesta (cuesta@lisa.u-pec.fr)

20 **Abstract.** We present a comprehensive study integrating satellite observations of ozone pollution, in situ measurements and chemistry transport model simulations for quantifying the role of anthropogenic emission reductions during the COVID-19 lockdown in spring 2020 over Europe. Satellite observations are derived from the IASI+GOME2 multispectral synergism, which provides particularly enhanced sensitivity to near-surface ozone pollution. These observations are first analysed in terms of differences between the average on 1-15 April 2020, when the strictest lockdown restrictions took place, and the same
25 period in 2019. They show clear enhancements of near-surface ozone in Central Europe and Northern Italy, and some other hotspots, which are typically characterized by VOC-limited chemical regimes. An overall reduction of ozone is observed elsewhere, where ozone chemistry is limited by the abundance of NO_x. The spatial distribution of positive and negative ozone concentration anomalies observed from space is in relatively good quantitative agreement with surface in situ measurements over the continent (a correlation coefficient of 0.55, a root-mean-squared difference of 11 ppb and the same standard deviation
30 and range of variability). An average bias of ~8 ppb between the two observational datasets is remarked, which can partly be

explained by the fact the satellite approach retrieves partial columns of ozone with a peak sensitivity above the surface (near 2 km of altitude).

For assessing the impact of the reduction of anthropogenic emissions during the lockdown, we adjust the satellite and in situ surface observations for withdrawing the influence of meteorological conditions in 2020 and 2019. This adjustment is derived
35   from the chemistry transport model simulations using the meteorological fields of each year and identical emission inventories. This observational estimate of the influence of lockdown emission reduction is consistent for both datasets. They both show lockdown-associated ozone enhancements in hotspots over Central Europe and Northern Italy, with a reduced amplitude with respect to the total changes observed between the two years, and an overall reduction elsewhere over Europe and the ocean. Satellite observations additionally highlight the ozone anomalies in the regions remote from in situ sensors, an enhancement
40   over the Mediterranean likely associated with maritime traffic emissions and a marked large-scale reduction of ozone elsewhere over ocean (particularly over the North Sea), in consistency with previous assessments done with ozonesondes measurements in the free troposphere.

These observational assessments are compared with model-only estimations, using the CHIMERE chemistry transport model. For analysing the uncertainty of the model estimates, we perform two sets of simulations with different setups, differing in the
45   emission inventories, their modifications to account for changes in anthropogenic activities during the lockdown and the meteorological fields. Whereas a general qualitative consistency of positive and negative ozone anomalies is remarked between all model and observational estimates, significant changes are seen in their amplitudes. Models underestimate the range of variability of the ozone changes by at least a factor 2 with respect to the two observational data sets, both for enhancements and decreases of ozone, while the large-scale ozone decrease is not simulated. With one of the setups, the model simulates
50   ozone enhancements a factor 3 to 6 smaller than with the other configuration. This is partly linked to the emission inventories of ozone precursors (at least a 30 % difference), but mainly to differences in vertical mixing of atmospheric constituents depending on the choice of the meteorological model.

1 Introduction

55 During boreal springtime of 2020, worldwide measures for curbing the spread of the COVID-19 virus have led to unprecedented and abrupt lockdowns in transportation (road, airplanes, and ships) and industry. These strong limitations drastically reduced the emissions of anthropogenic pollutants, inducing significant changes in atmospheric composition and air quality from local to worldwide scales, and particularly in regions such as China e.g. (Le et al., 2020) and Europe e.g. (Menut et al., 2020). Gkatzelis et al. (2021) provides an exhaustive overview of the current understanding of the influence of

60 emission reductions due to the lockdown throughout the world on atmospheric pollutant concentrations, where air quality is described in terms of nitrogen dioxide (NO_2), particulate matter ($PM_{2.5}$), ozone (O_3), ammonia, sulfur dioxide (SO_2), black carbon, volatile organic compounds (VOC), and carbon monoxide (CO).

Numerous efforts have been done for documenting and quantifying the reduction in the atmospheric abundance of primary air pollutants, such as nitrogen oxides NO_x ($NO+NO_2$) and sulfur oxides SO_x ($SO_2+H_2SO_4$), which are directly emitted to the

65 atmosphere. Satellite measurements derived from TROPOMI and OMI have shown reductions in NO_2 total columns of about 30-40 % over Chinese, European and North American source regions e.g. (Bauwens et al., 2020; Muhammad et al., 2020; Le et al., 2020) during the pandemic lockdown. Surface in situ measurements have also revealed clear reductions of NO_2 in the same order of magnitude e.g. (Ordóñez et al., 2020) and SO_2 e.g. (Le et al., 2020).

Modelling approaches based on the construction of emission inventories accounting for the changes in anthropogenic activities

70 have also shown consistent reduction of these primary pollutants (NO_x and SO_x) but also different regional regimes of either decreases or increases of the amounts of secondary pollutants, which are produced by photochemical reactions in the atmosphere e.g. (Le et al., 2020; Menut et al., 2020; Giani et al, 2020). This more complex picture is shown for secondary aerosols (organic or inorganic species) and tropospheric ozone.

An enhancement of the production of secondary particles has been linked to the alteration of atmospheric oxidizing capacity

75 during the pandemic lockdowns (Le et al., 2020). However, the total amount of aerosols, which partly have primary origin, has shown an overall reduction in terms of $PM_{2.5}$ (particle matter with aerodynamic diameter less than 2.5 μm) by roughly 5-10 % over Europe and 10-20% over China, during the 2020 springtime lockdown period.

On the other hand, ozone pollution either decreased or increased due to the reduction in the emissions of primary pollutants, depending on the photochemical regime. This has been shown by modelling and in situ observational studies, both in China

80 and Europe e.g. (Le et al., 2020; Shi and Brasseur, 2020 Giani et al., 2020; Souri et al., 2021; Mertens et al., 2021). Ozone decreased in rural areas, where photochemical production of ozone is controlled by the abundance of nitrogen oxides (thus a NO_x-limited regime), which concentrations clearly decreased during the pandemic lockdown. Ozone pollution clearly enhanced in urban areas (Ordóñez et al., 2020) and particularly in megacities (Sicard et al., 2020), as the reduction of NO_2 amounts strongly inhibited nighttime titration. The reduction of this dominant sink led to accumulation and therefore

85 enrichment of ozone, which prevailed over the reduction of ozone production associated with the lack of precursors. Although these processes have been remarked in previous works, the quantification of them is complex and it remains a challenge, as

well as the precise areas over which different regimes have prevailed. An additional major factor affecting the abundance of ozone, which adds complexity to its analysis, are the meteorological conditions. Using in situ surface observations and a predictive model of ozone variation against meteorological conditions, Ordóñez et al. (2020) suggested that clear sky

90   conditions and relatively high surface temperature in April 2020 as compared to previous years, induced intense ozone enhancements (in terms of daily 8-hour maximum) over Northern Europe, comparable and even larger than the enhancement associated with the pollutant emission changes linked to the pandemic lockdowns. Based on observation and meteorological analysis over the last seven years Deroubaix et al. (2020) suggested that the total oxidant concentrations ($O_x=O_3+NO_2$) decrease in Southwestern Europe while they remained unchanged in Northern Europe. Using a chemistry-transport model with emission

95   adjusted with respect to satellite measurements of NO_2 and formaldehyde, Souri et al. (2021) suggest a significant role of meteorological conditions but smaller than that associated with anthropogenic emissions changes during lockdowns (58% of the ozone enhancement, where it is 42% for meteorology change between 2020 and 2019). Moreover, a larger-scale study based on ozone measurements from in situ sondes and lidars remarked a reduction of free troposphere ozone across the northern hemisphere of about 7 % (4 ppb) due to worldwide activity reduction during spring and summer 2020 (Steinbrecht et al., 2020).

100   It is worth noting that none of these studies have used satellite measurements of ozone concentrations themselves as a complementary source of information.

The present work presents the first study integrating satellite ozone observations of lowermost tropospheric (LMT) ozone, surface in situ measurements and chemistry-transport modelling for analyzing the reductions and enhancements of ozone pollution over Europe associated with the COVID-19 lockdown of spring 2020. We use satellite measurements derived from

105   the IASI+GOME2 multispectral synergism which provides currently unmatched sensitivity to near-surface ozone (Cuesta et al., 2018). The sensitivity of this satellite retrieval shows a relative maximum for ozone around 2.2 km of altitude over land (while it is typically above 3 km for other standard satellite approaches, see details in Cuesta et al., 2013; 2018). It offers a full cloud-free spatial coverage, which is complementary to in situ measurements. We also use the chemistry-transport model CHIMERE (Menut et al., 2013; Mailler et al., 2017) for assessing the consistency of this model with respect to the observations

110   and to analyze the influence of meteorological conditions in 2020 as compared to 2019 (the year used as baseline or standard conditions in this study). We consider two different setups of the CHIMERE model, with different emission inventories and coupled with distinct meteorological models, for analyzing possible uncertainties in the simulations and the consistency with Air Quality e-Reporting database providing near-real-time air-quality measurements in Europe. Section 2 of the paper describes these datasets and the strategy used for their analysis. Section 3 presents the results, first in terms of total differences

115   between 2020 and 2019, secondly the influence of meteorological conditions and finally the impact of the COVID-19 lockdown on ozone pollution. Additional discussions and comparisons of the model simulations are also given in section 4. A last section 5 provides the conclusions of this work.

2 Multi-data integrated approach

Being a secondary and reactive pollutant, the analysis of tropospheric ozone is complex since it is influenced by many
competing factors. Tropospheric ozone sources and sinks are affected by multiple photochemical processes and non-linear
effects, which vary in time and space according to the availability of different precursors, either NO_x or VOC (originating
themselves from multiple anthropogenic and natural sources) and meteorological conditions. An integrated approach including
multiple datasets of different kinds is therefore valuable for better understanding the evolution of this pollutant. In the current
study, we use both satellite and in situ surface data to quantify the difference between the ozone pollution observed over Europe
in spring 2020 with respect to that in spring 2019, which is affected by both the lockdown reduction of pollutant emissions
and meteorological conditions. First, we verify the consistency of these observations with respect to the simulations from
CHIMERE with two different setups, for both meteorological fields and emission inventories. These two configurations of the
model are used for simulations of the two years, with a standard or "business as usual" inventory for 2019 and a modified
version in 2020 accounting for the lockdown conditions, called hereafter STD and COVID respectively. Second, we use the
chemistry-transport model with the same inventory (standard) for both years, 2020 and 2019, to derive a first order adjustment
for accounting for the influence on ozone pollution of the change in meteorological conditions between the two years. This
allows us to obtain an approximate estimate of the effects of the COVID-19 lockdown conditions on ozone pollution from the
two observational datasets (in situ and satellite). This is expressed by the following equation,

$$\Delta O_{3\,obs\&mod}^{covid} \approx O_{3\,obs}^{2020} - O_{3\,obs}^{2019} - \left(O_{3\,mod_{STD}}^{2020} - O_{3\,mod_{STD}}^{2019} \right) \qquad (1)$$

where "mod_{STD}" corresponds to simulated ozone with the standard or "business as usual" inventory. This adjustment does not
rely on any estimation of the variations in anthropogenic emissions during the lockdown. For simulations, the superscripts [2020]
or [2019] refer to the year of meteorological conditions that have been used. For observations, these superscripts indicate the year
when they were performed. The same equation stands for the adjustment of both surface measurements and satellite retrievals
(which are adjusted independently) but gridded at the location or horizontal resolution of each observation. The adjustments
for surface measurements and satellite retrievals use simulated ozone concentrations respectively at the surface and at the
lowermost troposphere (LMT, below 3 km of altitude, and these last ones are smoothed by the satellite averaging kernels). We
choose the model setup (C1 or C2, see section 2.3) that best agrees with respect to measurements in terms of the changes
between 2020 and 2019 (with models including the pandemic effects in 2020). The accuracy of this first order adjustment or
correction depends on the performance of the chemistry transport model to simulate ozone concentrations in "business as
usual" conditions as a function of meteorological conditions. It implicitly accounts for changes in biogenic emissions between
2020 and 2019 which are directly linked to meteorological conditions. However, this adjustment cannot account for the changes
in the chemical regimes (either NO_x-limited or VOC-limited) due to the changes in the abundance of ozone precursors nor
other complex chemical regimes (as modelled for parts of the Po valley, Thunis et al., 2021).

We will compare this synergetic "observational & model" estimate with the one derived from models only, based on the difference of ozone simulations with inventories COVID and STD and the meteorological conditions of 2020, as follows

$$\Delta O_3{}_{mod}^{covid} = O_3{}_{mod_{COVID}}^{2020} - O_3{}_{mod_{STD}}^{2020} \qquad (2)$$

155

In the current work, we mainly focus on the period from 1 to 15 April 2020 (and use 1-15 April 2019 as standard period) which corresponds to the 15-day period most perturbed emissions by the lockdown according to the COVID emission reduction factors from CAMS (https://atmosphere.copernicus.eu/covid-data-download). This work reports for example a reduction of -73 % of gasoline road transport for the 5 most populated countries in Europe (Germany, France, Great Britain, Italy and Spain,
160 that are also the largest contributors to the total European emission decreases), whereas it is -64 % and -66 % for the 15 days before and after (and then -54 % and -38 % for the two following fortnights). We also show some of the results for the whole month of April (2020 and 2019) to directly compare our estimates with those from previous works (Ordóñez et al., 2020; Souri et al., 2021) provided as monthly averages.

The following paragraphs describe briefly the datasets used by this approach.

2.1   IASI+GOME2 multispectral satellite observation of lowermost tropospheric ozone
165

The IASI+GOME2 satellite approach is designed for observing lowermost tropospheric ozone through the multispectral synergism of thermal infrared (IR) atmospheric radiances observed by IASI (Infrared Atmospheric Sounding Interferometer, Clerbaux et al., 2009) and ultraviolet (UV) earth reflectances measured by GOME-2 (Global Ozone Monitoring Experiment-2, EUMETSAT, 2006), according to the detailed description provided by Cuesta et al., (2013). Both instruments are onboard
170 the MetOp satellite series, and they both offer global coverage every day (for MetOp-A, B and C respectively around 09:30, 09:00 and 10:00 local time) with a relatively fine ground resolution (12 km-diameter pixels spaced by 25 km for IASI at nadir and ground pixels of 80 km × 40 km for GOME-2). IASI+GOME2 jointly fits co-located IR and UV spectra for retrieving a single vertical profile of ozone for each pixel. The horizontal resolution corresponds to that of IASI, using for each pixel the UV measurements from the closest GOME-2 pixel (without averaging).

175 The present work uses daily IASI+GOME2 multispectral observations of ozone available for clear sky and low cloudiness (pixel cloud fractions below 30%) and derived from the average of the retrievals using measurements from all available MetOp satellites (A, B and C for 2020 and A and B for 2019). The version of the algorithms used here is described and validated at global scale against ozone-sondes by Cuesta et al. (2018) (with a correlation of 0.85, a mean bias of -3% and a precision of 16%). The capacity to observe near-surface ozone with IASI+GOME2 has been shown by a good agreement against surface
180 in situ measurements of ozone for two major ozone outbreaks across East Asia and at daily scale (a correlation of 0.69, a weak mean bias of -5%, a precision of 20% and similar standard deviations for both datasets). Single-band approaches as those from IASI only were not able to observe such near-surface variability.

The IASI+GOME2 satellite product include vertical profiles of ozone, partial columns, averaging kernels (representing sensitivity of the retrieval to the true atmospheric state), error estimations and quality flags. Since 2017, global scale
185 IASI+GOME2 retrievals are routinely produced by the French data centre AERIS and they are publicly available (see https://www.aeris-data.fr and https://iasi.aeris-data.fr).

2.2   Surface in situ measurements

In this work, we use in situ surface measurements of O_3 and NO_2 from the European Air Quality e-Reporting (https://www.eea.europa.eu/data-and-maps/data/aqereporting-8). We only consider background stations of all categories
190 (urban, suburban, and rural). We analyze here daily and morning averages of measured surface concentrations and compared them with IASI+GOME2 ozone data and CHIMERE model simulations. A comparison shown in Table 2 and commented in section 3.1 suggests that a slight better agreement is found between daily averages of surface data (as compared to morning averages) and IASI+GOME2. This is likely linked to the fact that IASI+GOME2 retrievals show a relative maximum of sensitivity at about 2.2 km of altitude over land in mid-latitudes (see Cuesta et al., 2013). At this altitude and during the
195 overpass time of the MetOp satellites around 09:30 local time, the IASI+GOME2 approach likely measures ozone concentrations at the residual atmospheric boundary layer. We expect that the variability of these last ones is better represented by daily averages than morning surface concentrations, that have not yet been mixed vertically within the whole boundary layer. Therefore, most comparisons between IASI+GOME2 retrievals and surface concentrations consider daily averages of these last ones.

200   2.3   CHIMERE chemistry-transport model

CHIMERE is a state-of-the-art chemistry transport model widely used for studying atmospheric composition and forecast mainly at regional scale e.g. (Vautard et al., 2000; Honoré et al., 2008; Rouïl et al., 2009; Menut and Bessagnet 2010; Menut et al., 2015a; Marécal et al., 2015). It has been compared to numerous measurements, including meteorological variables and atmospheric chemical species (Menut et al. 2000; 2005, 2015b; Bessagnet et al., 2016; Vivanco et al, 2017). Regularly, new
205 versions of the model are proposed for a community of users (Menut et al., 2013; Maillet et al., 2017). Whereas ozone and nitrogen oxides are modeled as explicit species, other species such as particulate matter or VOCs are composed by several ensembles of families of species. Biogenic emissions are estimated with the MEGAN online model (Guenther et al., 2006), mineral dust with the scheme from Alfaro and Gomes (2001) and Menut et al., (2005b) and sea-salt with that from Monahan (1986).
210 In the present study, we use two different setups of CHIMERE with different anthropogenic emission inventories and meteorological conditions. This provides an estimation of the uncertainties of the ozone pollution simulations during the lockdown conditions, when varying these two key inputs. We also compare the two sets of simulations with respect to satellite and in situ observations, for identifying in which case there is a better match between observational and simulation datasets.

In both setups, CHIMERE simulations are run with horizontal resolution of 20×20 km² and 15 vertical levels from 998 to 300

215   hPa. Table 1 presents a brief description of the main elements of the two setups of the CHIMERE models.

2.3.1   Configuration 1 (C1) of CHIMERE

A first setup of CHIMERE, called hereafter C1 (Configuration 1), is based on the anthropogenic emissions from the HTAP
v2.2 inventory for 2010, on monthly basis (https://edgar.jrc.ec.europa.eu/htap_v2/, Janssens-Maenhout et al., 2015). The
original inventory is considered for STD simulations in 2019 and 2020, whereas for the COVID emissions in 2020 a relative

220   reduction for each activity sector (road transport, residential, industry, aviation, and shipping) is applied. The magnitude of the
decrease is estimated for the European domain based on the average for the five European most populated countries (Germany,
France, Great Britain, Italy, and Spain) of the CAMS COVID daily emission reduction factors for each sector, averaged over
the periods 1-15 April 2020 and 16-30 April 2020. Even though some differences occur in emission variability from country
to country, with Spain, Italy and France showing the strongest changes, while Great Britain and mostly Germany weaker ones,

225   we assume here a spatially homogeneous variation of emission factors over the whole domain. This corresponds to -73% (-
66%), -16% (-13%), -44% (-44%), +5% (+5%), -91% (-90%) and -19% (-18%) for emissions from road transport, power,
industry, residential, aviation and shipping sectors, for 1-15 (16-30) April 2020. According to CAMS, the COVID-19
restrictions led to a heterogeneous impact across different pollutants from industrial and residential sectors
(https://atmosphere.copernicus.eu/emissions-changes-due-lockdown-measures-during-first-wave-covid-19-europe).   For   the

230   industry sector, a smaller reduction is observed for non-methanic volatile organic compounds (NMVOC), NH_3 and SO_2 (mostly
emitted from food/beverage and chemistry industries, less affected by lockdown measures) with respect to other pollutants.
For the residential sector, only those pollutants mainly related to wood combustion processes (i.e., PM_{10}, $PM_{2.5}$, NH_3, NMVOC,
CO, biogenic CO_2 and CH_4) experienced a slight increase, while NO_x, SO_x, (and fossil fuel related CO_2) showed a modest
decrease. For that reason, CHIMERE C1 emissions for the COVID scenario consider the partitioning for industry between

235   NMVOCs, NH_3 and SO_x, and that for the residential sector between NO_x and SO_x, which are used within CAMS revised
inventory.

The C1 model configuration uses meteorological fields from the BOLAM e.g. (Buzzi et al., 1994) hydrostatic meteorological
model, whose boundary conditions are provided by the GLOBO e.g. (Malguzzi et al, 2011) hydrostatic general circulation
model. Both models are developed at CNR-ISAC (https://www.isac.cnr.it/dinamica/projects/forecasts/). Initial conditions of

240   BOLAM and GLOBO are taken each day at 0000 UTC from analyses of the NCEP/GFS model (Kalnay et al., 1996).
Climatological boundary conditions of trace gas concentrations from LMDz-INCA (Szopa et al., 2009; http://inca.lsce.ipsl.fr/).

2.3.2   Configuration 2 (C2) of CHIMERE

The second configuration (C2) of CHIMERE mainly corresponds to that used by Menut et al., (2020). The anthropogenic
emissions for the European domain are taken from EMEP (European Monitoring and Evaluation Programme, Mareckova et

245   al., 2019) emissions data released in 2019 (available for 2017). First, to estimate the reduction of all road transport emissions

for the COVID simulation, the "driving" dataset of the Apple company activity database was used. These data were used to apply a daily emissions reduction factor for each European country. Second, the emissions of the industrial and off-road sectors were establish using the same reduction factor but divided by two. Energy, agricultural and waste sectors were not changed. Finally, residential emissions are increased in order to account for the fact that people stay at home during the lockdown, but

250   by a fourth of the factor obtained from the Apple "driving" dataset. Discussions on the differences between the COVID-modified emissions for C1 and C2 are provided in section 4 in terms of NO_2 concentrations.

The C2 configuration considers meteorological fields from the WRF model v3.7.1 (Skamarock et al., 2007) forced by NCEP/GFS global fields (Kalnay et al., 1996). Boundary conditions are derived from CHIMERE simulations over a larger domain englobing North Africa and using anthropogenic emissions from CAMS (https://eccad3.sedoo.fr/#CAMS-GLOB-

255   ANT, Granier et al. (2019)).

3   Results

For better understanding the information provided by observations and simulations, the current multi-data analysis is presented in several steps. First, we focus on the total changes of ozone pollution between 2020 and 2019 (subsection 3.1), that are directly observed by in situ sensors and from space, and which we compare them with the corresponding amount simulated by

260   models. Then, we analyze the model-derived changes between these two years, but only associated with meteorological conditions (subsection 3.2). Finally, we compare changes of ozone pollution only linked with the pandemic lockdown conditions, estimated from models and observations (subsection 3.3). The originality of these results resides in the use of in situ and satellite observational estimates of the changes in ozone pollution associated the lockdown conditions $\Delta O_{3}{}^{covid}_{obs\&mod}$, that are adjusted for avoiding meteorology effects. This adjustment is derived from the model using business as usual emissions

265   and thus avoiding the ambiguities associated to the estimation of anthropogenic emissions during the lockdown period.

Additional comparisons of the two model setups (C1 and C2) are also provided for better understanding the differences between these simulations and their agreement with respect to observations (section 4). These comparisons allow the identification of key elements that influence the accuracy of the model and the configuration that better match the observations.

3.1   Changes in ozone pollution in 2020 with respect to 2019

270   #### 3.1.1   Satellite and in situ surface measurements

The first step of our study consists of analyzing all available datasets in terms of the changes in ozone pollution over Europe between the pandemic lockdown period in 2020 (focused here on April) with respect to the same period during the previous year (this difference is hereafter called $\Delta O_3{}^{2020-2019}$). Figure 1 shows a comparison between the two observational datasets averaged over the periods 1-15 and 1-30 April. The first 15 days of the month show the most pronounced changes between the

275   2 years and the monthly average is also shown for comparison with previous works. Figures 1b and 1d only consider in situ

surface measurements coincident in time and space with satellite data. A good agreement is shown in terms of regional ozone patterns between IASI+GOME2 satellite data and in situ surface measurements. Both datasets clearly show similar structures of positive and negative anomalies. Ozone enhancements in 1-15 April 2020 with respect to 2019 are seen both by satellite and surface data over Northern and Eastern France, Western and Southern Germany, Northern Italy, and Southwest England

280 (Figs. 1a-b). Ozone photochemistry in these regions is typically dominated by VOC-limited conditions, remarked both in standard situations (e.g., Beekmann and Vautard, 2010, Wilson et al., 2012) and during the pandemic lockdown (e.g., Menut et al., 2020; Gaubert et al., 2021). Both measurements also show clear ozone reductions in 2020 for less urbanized regions typically characterized by NOx-limited chemical conditions: Spain, Southern Italy, Poland, and Western England. A near neutral or intermediate behavior is seen over Eastern Germany (in consistency with Beekmann and Vautard (2010)), with

285 rather limited reductions of ozone both for IASI+GOME2 and surface data. When considering averages over the whole month of April (the period averaged in other studies in literature, Figs. 1c and 1d), we also find a clear consistency between surface and satellite observations. Both datasets show similar horizontal patterns of positive and negative anomalies, with less pronounced ozone enhancements in central Europe and Northern Italy than for the average over the first 15 days of the month. Moreover, the ozone increase over France has a more limited horizontal extent, with prevailing reductions of ozone in central

290 France.

In quantitative terms, scatterplot comparisons of co-located IASI+GOME2 and in-situ data in time and space are presented in Fig. 2 (in terms of differences in daily ozone concentrations between 2020 and 2019 on 1-15 and 1-30 April). Colors represent the number of occurrences for intervals of 2 ppb of ozone in both axes. For the period 1-15 April (Fig. 2a), the correlation coefficient between these datasets is 0.55 while the standard deviation of both datasets is practically the same and the root

295 mean squared (RMS) difference is 11.8 ppb. As the variability of the ozone anomalies is smaller for the monthly average (Fig. 2b), the correlation coefficient is moderately lower (0.46), and the RMS difference is reduced (10 ppb). There is an average difference or bias (of 8.6 ppb for 1-15 April) for the average ozone concentration changes, with lower values for the satellite retrievals than those for in situ data. This bias may partially come from the differences in the altitude of the measurements: in situ data are surface measurements whereas IASI+GOME2 measurements are lowermost tropospheric ozone columns. The

300 satellite retrieval of this partial column is typically most sensitive around 2.2 km above sea level over land (quantified over Europe by Cuesta et al., 2013). Therefore, the negative bias for IASI+GOME2 with respect to surface concentrations may suggest that ozone concentrations at atmospheric layers roughly ~2 km above surface level decreased more than at the surface with respect to the same periods in 2019. This could be explained by several reasons such as a larger sensitivity to emission changes at the surface than at higher altitudes, differences in sampling time and also by the fact that satellite measurements

305 sample air masses of both the boundary layer and free troposphere, where ozone concentrations may have had different variations between 2019 and 2020. Moreover, surface ozone concentrations are directly affected by titration with NO; its impact on ozone columns up to 3 km is expected to be lower. Since the degree of freedom for the LMT partial columns is generally lower than 1 (typically 0.35 over land in Europe), IASI+GOME2 retrievals could also have some influence of the a priori concentrations.

310   The observational study from Steinbrecht et al., (2020) shows a clear reduction of ozone concentrations of -6 to -9 % in the free troposphere (1-8 km of altitude) in the extratropical northern hemisphere, likely associated with the reduction of anthropogenic emissions at large scale during the pandemic lockdown in 2020. This large-scale reduction of ozone concentrations in the free troposphere associated with the lockdown conditions in 2020 is consistent with the negative difference of LMT ozone satellite retrievals (capturing the variability of both ozone in the boundary layer and the free

315   troposphere) with respect to surface ozone concentrations.

    Figure 3 presents an additional analysis of the changes in ozone pollution between 2020 and 2019, but in terms of the maximum daily 8-hour average (MDA8) of surface ozone. This quantity is often used as indicator of air quality and it is considered as metrics for ozone pollution in the previous studies used for comparison in the next sub-section (i.e., Ordóñez et al. 2020; Souri et al., 2021). We notice rather similar horizontal patterns of positive and negative anomalies between the two years in terms

320   of MDA8 ozone concentrations over most of Europe (central Europe, France, Spain and Italy, Fig. 3a-b) as compared with daily averages (Fig. 1b, d). The main qualitative difference is seen in the 1-15 April period over the neutral regime region of Eastern Germany and Southern Poland, where enhancements are seen in terms of MDA8 ozone while daily averages show reductions. In quantitative terms, the MDA8 ozone concentrations changes are clearly larger than for daily averages, by about a factor ∼2 (see Table 3 for targeted regions). These differences are probably linked to the fact that daily averages also account

325   for low ozone concentrations during the night and therefore their variability is reduced with respect to daily maxima expressed here as MDA8.

    In relative terms, Figure 3b shows very similar horizontal patterns of positive and negative anomalies as compared with the estimate from Souri et al., 2021 (Fig. 9 of this work). The average ozone change over the Central Europe region (43-52°N 0-20°E) is moderately larger in the present work (11.0 %, see Table 2) than that from Souri et al. (2021; i.e., 7.4%), which can

330   partly stem from the choice of surface stations considered in study. The ozone changes in April 2020 derived by Ordóñez et al., 2020 (Fig. 1 of this work, e.g., +12 to +22 % in the Benelux) are also consistent with the present work (16 % in the Benelux area, see Table 2). However, ozone enhancements extent further east (also over Eastern Germany and Poland) in the estimations of Ordóñez et al. 2020 as compared to Fig. 3b. This can partly come from the fact that Ordóñez et al. 2020 use an average of 2015-2019 as "standard" conditions, while only 2019 is considered here.

335   **3.1.2   Model simulations**

    When it comes to model-derived differences of surface ozone concentrations between 2020 (using COVID emissions) and 2019 for 1-15 April, we remark notable differences depending on the configuration of CHIMERE (see Fig. 4). With both setups, the model simulates ozone enhancements in 2020 with respect to 2019 over Northeastern Europe and Northern Italy, and reductions over Spain and the Atlantic. However, clear differences between the model configurations are seen over France,

340   where CHIMERE C2 suggests very limited changes (mainly small reductions) and CHIMERE C1 an enhancement, in consistency with most surface in situ measurements and IASI+GOME2 data. Similarly, CHIMERE C1 shows ozone reductions over the North Sea, Southern Italy and Central-eastern Mediterranean in agreement with IASI+GOME2, whereas

enhancements are shown by CHIMERE C2. Over Poland, limited changes are depicted by the model in the C1 configuration and a clear enhancement according to C2, whereas both observations (in situ and satellite) depict clear reductions in 2020 with

345   respect to 2019. The scatterplots of Fig. 5 show a better overall agreement for CHIMERE C1 with respect to in situ data than for CHIMERE C2 (with correlation coefficients of e.g., 0.67 and 0.44 for C1 and C2, respectively, in 1-15 April). However, both configurations of the models clearly underestimate the variability of the ozone changes in spring 2020 with respect to the previous year, as compared to in situ measurements (larger by more than a factor ∼2). Whereas $\Delta O_3^{2020\text{-}2019}$ observed at the surface range from roughly -12 to +12 ppb in terms of daily averages, simulated values only spread from -6 to +6 ppb. The

350   range of values of IASI+GOME2 has the same amplitude as compared to in situ data but shifted towards smaller values (-20 ppb to +5 ppb). Similar features are remarked for the average over the whole month of April and 1-15 April, with larger enhancements for this last one.

Generally, simulations (both C1 and C2) show total anomalies in 2020 (with respect to 2019) that are only partially associated with the regions of typical "NOx-limited" and "VOC-limited" chemical regimes. On the other hand, observations from both

355   in situ sensors and satellite do show clearer similarities between the typical regimes (in the regions where both datasets are available) and ozone anomalies during the pandemic lockdown. This might be linked to a large influence of meteorological conditions in the models, as compared to lockdown induced emission changes. Still another reason for these differences could be that boundary conditions for CHIMERE simulations (both C1 and C2) do not account for the changes in anthropogenic emissions linked with the pandemic in 2020 (for 2019 and 2020, the same climatology is used for C1 and the same emission

360   inventories for C2). This would lead to a positive bias in simulated differences if part of the observed decrease at the free troposphere (by Steinbrecht et al., 2020) affected the surface. Overall, the differences between the two model setups, and also with respect to observations highlight the complexity to simulate the effect of the changes in ozone concentrations due to changes in anthropogenic emissions, as occurred during the lockdown. In the following subsections 3.2 and 3.3, we use CHIMERE C1 simulations to derive the adjustments for observations as they show a better correlation to surface observations

365   than those from CHIMERE C2 (Fig. 5). Further discussions on the causes of the differences between C1 and C2 simulations are provided in section 4.

3.2   Changes in ozone pollution associated with meteorological conditions

Figure 6c shows the changes of MDA8 surface ozone in April 2020 with respect to April 2019 associated with meteorological conditions, derived with the CHIMERE C1 model and keeping the same anthropogenic emissions for the two years (2020

370   STD-2019). It shows that meteorological conditions in 2020 induced a clear enhancement in ozone concentrations over continental Europe almost everywhere north of 44°N ranging from 5 % (over Eastern France and Southern Italy) to 10 % (Belgium, Northern Germany, and Northern Poland) and a maximum of about 15 % (a band from Benelux to Northern Italy), as well as a reduction of roughly -5 % over Spain. These estimates are consistent with the two previously mentioned studies. The locations of the positive and negative anomalies of ozone changes associated with meteorological conditions are in clear

375   agreement with the estimations for this same quantity (meteorological effects only) from Souri et al., 2021 (see middle panel

of Fig. 11 of this paper) and north of 44°N for Ordóñez et al., 2020 (examining the differences between the lower panels of Fig. 1 of this paper). In quantitative terms, our estimate shown in Fig. 6c agrees well with that for Ordóñez et al. (2020) over France, Belgium, Germany, and Italy. Ordóñez et al., (2020) derives 5, 10 to 13 %, 10 to 12% and 3% for these 4 countries, according to the differences between observed and meteorology-adjusted changes reported in Table 1 of this paper. For central

380 Europe, we estimate here an averaged enhancement of MDA8 ozone associated with meteorological conditions of ~8 %, while Souri et al., (2021) derived an average of ~1.7 % for the same area. Likewise, the total change of MDA8 ozone over this area seems to be underestimated by the Souri et al. (2021) model (~3.7 %) as compared to surface in situ measurements (~7.4 % in their study and ~8 % in ours). Moreover, Souri et al. (2021) estimate a reduction of ozone linked to meteorological/biogenic emissions effects over Southern Europe of roughly -5% (in agreement with Fig. 6c).

385 In the period 1-15 April, our estimates show that meteorological conditions induce an enhancement MDA8 surface ozone of 14 % over Central Europe (Fig. 6a), which is ~6 % larger than the average over the whole month. This suggests that during the first 15 days of the month the largest reduction of anthropogenic emissions (according to CAMS) is concomitant with a larger European ozone production north of 44°N associated with meteorological conditions.

3.3   Impact of COVID19 lockdown of spring 2020 in ozone pollution

390 Figures 6b and 6d show net changes of ozone pollution in terms of surface MDA8 concentrations only associated with the pandemic lockdown, which are derived from in situ measurements after withdrawing the influence of meteorological conditions (using Eq. 1). We remark that ozone enhancement over a band from Benelux to Northern Italy (green rectangle in Fig. 3a) is clearly less pronounced, but it is still significant when excluding meteorological effects. Over this area, we estimate a MDA8 surface ozone enhancement related to the lockdown during the month of April of ~3 % (Table 3) and a maximum

395 value over Northeastern Italy of ~20 %. Moreover, ozone changes derived from adjusted surface observations are negative anomalies over the center of France and part of center of Germany (Fig. 6b, d), while total observed changes were positive in the 1-15 April period (Fig. 3a).

An overall agreement is found in the positive and negative patterns between Fig. 6d and those depicted by Ordóñez et al., (2020) and Souri et al., (2021). In the 3 estimates excluding meteorological effects, a net enhancement of surface ozone is seen

400 across a region extending from Southern England, Benelux, Northeastern France/Southwestern Germany, and Northern Italy. Our estimate of the ozone enhancements over these regions is rather consistent with that estimated by Ordóñez et al. (2020) and Souri et al. (2021), ranging from ~3 to ~8 % (according to Figures 1 and 11 respectively of these papers). On the other hand, a net reduction of MDA8 ozone concentrations is derived over Southwestern and Northeastern Europe of -7 and -8 %, respectively (see Table 4). For these regions, Ordóñez et al. (2020) roughly estimate a reduction -2 % to -7 % whereas these

405 values are near zero for the model-derived values from Souri et al. (2021).

In the period 1-15 April, the net ozone enhancement associated with the lockdown is clearly larger over Central Europe (~9 % larger and in the band from Benelux to Northern Italy ~10 % larger) than in the average over the whole month. It also extends further east and south (see Figs. 6b and 6d, Tables 3 and 4). The greater net increase of ozone pollution during the first

15 days of the month is consistent with the occurrence of the greatest perturbation of the anthropogenic activities, as suggested

410 by the revised inventories of CAMS (remarked in section 2). In addition, the net reductions of ozone over Northeastern Europe show slightly less pronounced values in this period (-4 %) than over the whole month (-8 %).

Figure 7 presents the changes of daily average ozone concentrations associated with the lockdown derived from IASI+GOME2 satellite retrievals, in situ measurements and the CHIMERE model (C1 and C2 setups). We notice that the spatial patterns of the surface ozone anomalies are qualitatively similar for daily averages (Fig. 7b) and MDA8 (Fig. 6b), while their amplitude

415 are roughly a factor 2 smaller for daily averages (see Table 2). The satellite-derived estimate of lowermost tropospheric ozone changes during 1-15 April 2020 (Fig. 7a) is clearly consistent with that derived from surface in situ measurements (Fig. 7b), both adjusted for avoiding the effects of meteorological conditions. The location of the positive and negative anomalies of ozone satellite retrievals is like those of total changes between 2020 and 2019 (Fig. 1a). Although, as for surface concentrations, the satellite-derived amplitude of the ozone enhancements linked to the lockdown over Central Europe is

420 clearly less pronounced than the total changes. Clear lockdown-derived enhancements of LMT ozone retrievals are seen over the Rhone Valley (reaching the Mediterranean), Northern and Eastern France, the Po Valley and Eastern England.

Satellite data offer an extended geographical coverage with respect to surface in situ measurements. We remark a clear continuity in the ozone change patterns in countries only partially or not sampled by in situ sensors, such as those of Eastern Europe (from Latvia to Greece, with reductions of roughly -13 ppb), other regions as Check republic, Austria, Southern France,

425 Southern Italy, parts of Spain and over the oceans. IASI+GOME2 depicts clear net reductions in ozone concentrations in 2020 south of the Mediterranean and part of the Atlantic west of France (respectively -11 and -8 ppb) and more important decreases over the North Sea (-21 ppb).

Model-only estimations of the impact of the pandemic lockdown on ozone pollution (Fig. 7c-d) show both qualitative similarities and differences with respect to those using observations. Similar patterns of ozone enhancements up to ~5 ppb are

430 remarked over Eastern England, Northern France, the Benelux and Northern Italy for observation-derived methods and CHIMERE C1 (Fig. 7c). This last one suggests a net ozone enhancement over the part of the Mediterranean Sea located south of France, which is associated with the reduction of shipping activities in this area and is also clearly observed by IASI+GOME2. On the other hand, the model with the C1 setup simulates enhancements of ozone pollution over Western England and the North Sea, where observations suggest reductions. Over Germany and Poland, observations suggest the

435 predominance of ozone reductions while CHIMERE C1 indicates a moderate ozone enhancement (1-2 ppb). We can also notice that C1 simulations overestimate the ozone enhancements over Germany and England and underestimates the ones over Northern Italy, as compared to the two observational datasets. This can be partly attributed to the assumed homogenization of the lockdown conditions for these countries, whereas actual restrictions in Germany and England were less strict than in Italy. In qualitative terms and over land, the horizontal distribution of positive and negative anomalies associated with the lockdown

440 is quite similar for both CHIMERE setups (C1 and C2), but the absolute values are quite different (Fig. 7c and 7d). The amplitudes of the anomalies are approximately a factor 3 to 6 larger for C1 than those for C2. Ozone enhancements for C1 reach ~6 ppb over Benelux and the Po Valley, while they are of about ~1 ppb for C2. The net ozone reduction over the

Southern Mediterranean is -4 ppb and -1 ppb for C1 and C2, respectively. The origin of these differences in these two sets of simulations is discussed in the following section.

445 **4 Discussions and additional comparisons of the two model setups**

A fair qualitative consistency is remarked between observations (in situ and satellite) and CHIMERE datasets with respect to the regions of ozone enhancements and reductions associated with the pandemic lockdown conditions. Ozone increased over more urbanised regions with large NO_x emissions, as Central Northern Europe and the Po Valley, and mainly decreased far from NO_x hotspots where night-time titration plays a less important role in the surface ozone daily balance. A significant 450 model/observations difference is found over Eastern Germany and Poland, where the model shows moderate ozone enhancements while both observations suggest clear reductions. This might be linked to the difficulty to accurately simulate neutral chemical regimes, with competing terms of ozone production and sinks, requiring a larger precision of the emission inventories and other factors affecting the abundance of active chemical species.

Significant differences are seen in the amplitudes of the positive and negatives anomalies of ozone pollution in spring 2020. 455 On the one hand, in situ and satellite observations agree in terms of the total range of changes of ozone (both between 2020 and 2019 and adjusted for meteorological effects) of about ~25 ppb between maximum positive and minimum negative anomalies over land, with satellite data shifted by ~8 ppb towards smaller values (which can partly be linked to the altitude of sensitivity of these retrievals). On the other hand, CHIMERE underestimates the amplitude of these changes in ozone pollution (with the largest range for variability of ~12 ppb for C1), with respect to observations. This limited variability of ozone with 460 respect to observations is also found for the chemistry-transport model of Souri et al., (2021) that uses adjusted European emissions of NO_X and VOC with respect to satellite data. Particularly, we notice underestimations of the absolute amplitude of negative anomalies which are seen over land and over ocean with respect to satellite data. This may be partly explained by the fact that boundary conditions of the models only account for the changes in ozone concentrations and its precursors associated with the pandemic lockdown over Europe, but other changes at global scale are not considered. Nevertheless, the 465 observational study of Steinbrecht et al. (2020) suggests that these last ones correspond to a significant ozone reduction in the free troposphere across the whole northern hemisphere in spring and summer 2020 (-7 % or -4 ppb over the northern extratropics). We likely expect this large-scale ozone reduction to be more pronounced at the beginning of this period (e.g., beginning of April 2020) as it is a period with more generalized and severe lockdowns over Europe and North America, as well as the last part of the lockdown over China and some restrictive measures over South Korea and Japan. Moreover, the 470 ozone reduction in spring/summer 2020 is more noticeable near the North Sea (Lerwick) than for south of France (Haute Provence) near the Mediterranean, as remarked with the IASI+GOME2 retrievals over these two oceanic regions (Fig. 1a, 7a). When it comes to the amplitude of the ozone anomalies associated to the pandemic lockdown, clear differences are remarked between for the two CHIMERE configurations (Fig. 7c-d). A key factor explaining the larger amplitude of the ozone anomalies for C1 as compared to C2 is linked to the abundance of ozone precursors. Indeed, significant differences between C1 and C2

475 are seen both in terms of NO_2 concentrations in absolute values for a given year in standard conditions (2019), differences between 2020 and 2019 and between urbanized/rural regions (see Fig. 8 and Table 5). In 2019, NO_2 concentrations are larger for C1 than C2, by a factor ~3 over a large heterogenous area as the Benelux to Northern Italy band and only by ~50 % for a megacity as Paris. In both cases, these simulated concentrations are lower than those measured by in situ measurements (~20 % larger than values for C1, see Table 5). For all in situ stations, the mean biases (root-mean-squared differences) of coincident

480 NO_2 concentrations simulated in 2019 are quite significant (around -5 (6) ppb for C1 and -6 (8) ppb for C2) and similar for both model setups.

We also find larger changes of NO_2 abundances in absolute values between 2020 and 2019 for C1 than for C2, both for the band from Benelux to Northern Italy and Paris (by a factor ~4 and ~5 respectively). This likely explains most of the differences in the simulated changes of O_3 associated with the lockdown conditions in 2020. The larger O_3 precursors emissions

485 changes during the lockdown considered for C1 clearly manifest as larger changes in the abundance of O_3, as compared to C2. When comparing with in situ measurements of $\Delta NO_2^{2020-2019}$, the measured reduction over a horizontally homogenous hotspot as Paris clearly matches C1, while it is underestimated by C2 (by a factor ~5). Inversely, we remark an agreement for C2 for averages over a heterogenous large area (as the Benelux to Northern Italy band) while it is overestimated in absolute values by C1 (by a factor ~4). Therefore, the agreement between simulated and measured $\Delta NO_2^{2020-2019}$ clearly depends on the criteria

490 and the horizontal homogeneity of the abundancies over the area considered in the comparison.

These large differences in the simulated NO_2 concentrations are partly linked to the inventories used in each setup. The configuration C1 is based on emission inventories estimated for 2010 (by HTAPv2.2, on monthly basis) and C2 on an inventory calculated for 2017 (by EMEP and with a seasonal modulation). A sustained negative trend for NO_2 concentrations observed over Europe between 2010 and 2017 (e.g., Pazminio et al., 2021) suggests a positive bias for the inventory used for C1 as

495 compared to C2. This trend is ~30 % in France, slightly higher in Italy or Belgium and smaller for other countries as Germany and Poland (~13%, see EMEP database, https://www.ceip.at/webdab-emission-database/emissions-as-used-in-emep-models). Other factors significantly affecting simulated concentrations of ozone and its precursors are clearly linked to the meteorological fields used by the model. Indeed, vertical mixing withing the atmospheric boundary layer can largely modify the concentrations of any atmospheric constituent at surface level. We assess its role by comparing total atmospheric columns

500 of NO_2 integrated in the vertical for C1 and C2 (Figure 9), which are not directly affected by vertical mixing. We notice that both total columns in 2019 and differences between the two years (Fig. 9) are much closer between C1 and C2 than surface concentrations (Fig. 8). Total columns of NO_2 in 2019 are only ~50 % larger for C1 than for C2, both in large regions and megacities (such as the Benelux to Northern Italy band and Paris). This magnitude of difference can be explained by the differences in the years of the emission inventories and remaining differences in the estimations by HTAP and EMEP. We

505 notice as well that the change of abundance between the two years $\Delta NO_2^{2020-2019}$ is a factor 2 larger for C1 and C2, which can stem from how emissions are modified to account for the pandemic lockdown in each of the setups.

An additional comparison between the meteorological fields used in C1 and C2 is shown in Figure 10, in terms of changes in surface pressure and temperature between 2020 and 2019. Both simulations show higher surface pressure from the Atlantic

northwest of France to Italy, associated with anticyclonic conditions prevailing in 2020 (Fig. 10a-b). The enhancement of
510   surface pressure in 2020 over the Atlantic and France is larger for C2 than for C1. Surface temperature changes between 2020
and 2019 are also similar for C1 and C2, except over France where meteorological conditions considered in C1 suggest a clear
temperature enhancement in 2020 with respect to the previous year, while those for C2 only show a slight increase and only
located in southwestern part of this country. These regional differences in meteorological conditions over France may partly
explain (if one accepts a positive temperature-ozone relationship, as often observed during summer) why C1 simulates a clear
515   ozone enhancement all over this country in 2020 with respect to 2019 and C2 shows a very limited change in ozone abundance
in this case (see Fig. 4).

5   Conclusions

We have presented a comprehensive analysis using in situ and satellite measurements of ozone as well as chemistry-transport
modelling tools of the changes in ozone pollution over Europe associated with the COVID-19 pandemic lockdown of
520   springtime 2020. To the authors' knowledge, this is the first time that satellite direct observations of lowermost tropospheric
ozone are used in such a multi-data analysis. While satellite observations of ozone show a fairly good agreement with respect
to in situ surface measurements of ozone across Europe in the regions where both are available, only satellite data provide full
horizontal coverage over the region both over land and ocean (at 0.25°×0.25° horizontal resolution). The observations quantify
the changes of ozone pollution in 1-15 April 2020 with respect to the same period the previous year, thus the 15-day period
525   when the lockdown measures modified the most anthropogenic activities over the continent. Comparisons are also performed
for the whole month of April 2020.

An additional original aspect in the present analysis is the adjustment of both in situ and satellite observations for accounting
for the main effects of the changes in meteorological conditions between the two years. This adjustment is derived from the
chemistry-transport model CHIMERE using the meteorological conditions of each year but the same standard (business as
530   usual) anthropogenic emissions. This method relays on the model accuracy in standard conditions and it neglects possible
feedbacks between meteorological conditions and photochemical regimes. The influence of biogenic emissions is accounted
for by the method, as these sources are derived according to the meteorological conditions. The adjustment can be directly
applied to both in situ and satellite data, with good consistency with respect to other independent approaches used for the same
kind of adjustment of surface in situ data (Ordóñez et al., 2020) or using integrated process rates derived from a chemical
535   transport model (Souri et al., 2021).

Based on meteorology-adjusted satellite and in situ observations, the present work provides a comprehensive estimate of
change in ozone pollution associated with the pandemic lockdown. It shows a significant enhancement of ozone in the VOC-
limited regions of central and northern Europe and the Po Valley, pointed out previously by models and in situ surface data
(e.g. Menut et al., 2020; Ordóñez et al., 2020; Souri et al., 2021) that overlaps with the large-scale reduction of ozone over the

540   whole continent (seen in the free troposphere by ozone sonde measurements, Steinbrecht et al., 2021) and clearly put in evidence over the ocean (Atlantic, North and Mediterranean seas).

We compare these observation-based estimations with model-only estimates derived by changing emissions according to the reductions in anthropogenic activities estimated for the lockdown period. For this, we use two different model configurations, with distinct emissions in standard and COVID-19 conditions and meteorological fields. These two model-based estimates

545   provide similar regional patterns of enhancements and reductions of surface ozone, but clearly different magnitudes (by a factor 3 to 6). This is mainly explained by marked differences in vertical mixing within the atmospheric boundary layer, according to the use of two different meteorological models, as well as the year for which the emission inventories were estimated (one simulation uses an inventory from 2010 and the other from 2017) and different assumptions in variations of anthropogenic emissions during the lockdown. As compared to measurements, both configurations underestimate the

550   amplitude of the positive and negative anomalies. However, the configuration that shows amplitudes closer to those observed are the ones whose abundances of ozone precursors (e.g., NO_2) in absolute terms (in standard conditions and changes during the lockdown over homogenous hotspots) are closer to those observed by in situ sensors. The differences between the simulations using two different model setups, and with respect to observations highlight the complexity to simulate the effect of the changes in ozone concentrations due to changes in anthropogenic emissions, as occurred during the lockdown.

6   Acknowledgements

Authors are grateful for the financial support of Centre National des Etudes Spatiales (CNES, the French Space Agency) via the "SURVEYPOLLUTION" project from TOSCA (Terre Ocean Surface Continentale Atmosphère), the Université Paris Est Créteil (UPEC) and the Centre National des Recherches Scientifiques-Institut National des Sciences de l'Univers (CNRS-INSU), for achieving this research work and its publication.

We warmly acknowledge the French atmospheric datacentre AERIS (www.aeris-data.fr) for supporting the production of IASI+GOME2, the European Air Quality e-Reporting for in situ surface measurements of ozone and nitrogen dioxide, EUMETSAT for GOME-2 level 1 data (provided by the NOAA CLASS data portal), Copernicus Atmosphere Monitoring Service (CAMS) for the revised inventory of anthropogenic emissions during the COVID-19 lockdown in Europe and Apple transport data. IASI is a joint mission of EUMETSAT and CNES. We thank the Institut für Meteorologie und Klimaforschung (Germany) and RT Solutions (USA) for licences to use respectively the KOPRA and VLIDORT radiative transfer models. We also thank Z. Cai from the Chinese Academy of Sciences (China) and X. Liu from Harvard-Smithsonian (USA) for their support to produce IASI+GOME2 data.

570 **7   References**

Alfaro, S.C., Gomes, L. Modeling mineral aerosol production by wind erosion: emis- sion intensities and aerosol size distribution in source areas. J. Geophys. Res. 106 (18) (075–18, 084), 2001.

Bauwens, M., S. Compernolle, T. Stavrakou, J.F. Müller, J. Van Gent, H. Eskes, P. F. Levelt, R. van der A, J. P. Veefkind, J.
575 Vlietinck, Huan Yu, C. Zehner. Impact of coronavirus outbreak on NO2 pollution assessed using TROPOMI and OMI observations. Geophys. Res. Lett., 47(11), e2020GL087978, 2020.

Beekmann, M. and Vautard, R. A modelling study of photochemical regimes over Europe: robustness and variability. Atmos. Chem. Phys., 10(20), 10067-10084, 2010.

Bessagnet, B., Pirovano, G., Mircea, M., Cuvelier, C., Aulinger, A., Calori, G., Ciarelli, G., Manders, A., Stern, R., Tsyro, S.,
580 García Vivanco, M., Thunis, P., Pay, M.T., Colette, A., Couvidat, F., Meleux, F., Rouïl, L., Ung, A., Aksoyoglu, S., Baldasano, J.M., Bieser, J., Briganti, G., Cappelletti, A., D'Isidoro, M., Finardi, S., Kranenburg, R., Silibello, C., Carnevale, C., Aas, W., Dupont, J.C., Fagerli, H., Gonzalez, L., Menut, L., Prévôt, A., Roberts, P., White, L.. Presentation of the EURODELTA III intercomparison exercise - evaluation of the chemistry transport models' performance on criteria pollutants and joint analysis with meteorology. Atmos. Chem. Phys. 16, 12667–12701. https://doi.org/10.5194/acp-16-12667-2016, 2016.

585 Buzzi, A., Tartaglione, N., Malguzzi, P. Numerical simulations of the 1994 Piedmont flood: Role of orography and moist processes. Monthly Weather Review, 126(9), 2369-2383, 1998.

Clerbaux, C., Boynard, A., Clarisse, L., George, M., Hadji-Lazaro, J., Herbin, H., Hurtmans, D., Pommier, M., Razavi, A., Turquety, S., Wespes, C., and Coheur, P.-F.: Monitoring of atmospheric composition using the thermal infrared IASI/MetOp sounder, Atmos. Chem. Phys., 9, 6041–6054, doi:10.5194/acp-9-6041-2009, 2009.

590 Cuesta, J., M. Eremenko, X. Liu, G. Dufour, Z. Cai, M. Höpfner, T. von Clarmann, P. Sellitto, G. Foret, B. Gaubert, M. Beekmann, J. Orphal, K. Chance, R. Spurr and J.-M. Flaud. Satellite observation of lowermost tropospheric ozone by multispectral synergism of IASI thermal infrared and GOME-2 ultraviolet measurements over Europe, Atmos. Chem. Phys., 13, 9675–9693, 2013.

Cuesta J., Kanaya, Y., Takigawa, M., G. Dufour, M. Eremenko, G. Foret, Miyazaki, K., M. Beekmann, Transboundary ozone
595 pollution across East Asia: daily evolution and photochemical production analysed by IASI + GOME2 multispectral satellite observations and models, Atmos. Chem. Phys., 18, 9499-9525, https://doi.org/10.5194/acp-18-9499-2018, 2018.

Deroubaix, A., G. Brasseur, B. Gaubert, I. Labuhn, L. Menut, G. Siour, P. Tuccella. Response of surface ozone concentration to emission reduction and meteorology during the COVID-19 lockdown in Europe, Meteorol Appl., 2021.

Gaubert, B., Bouarar, I., Doumbia, T., Liu, Y., Stavrakou, T., Deroubaix, A., Sabine Darras, N. Elguindi, C. Granier, F. Lacey,
600 J.-F. Müller, X. Shi, S. Tilmes, T. Wang, Brasseur, G. P. Global changes in secondary atmospheric pollutants during the 2020 COVID-19 pandemic. J. Geophys. Res. Atmos., 126(8), e2020JD034213, 2021.

Giani, P., Castruccio, S., Anav, A., Howard, D., Hu, W., Crippa, P. Short-term and long-term health impacts of air pollution reductions from COVID-19 lockdowns in China and Europe: a modelling study. The Lancet Planetary Health, 4(10), e474-e482, 2020.

605   Gkatzelis, G. I., J. B. Gilman, S. S. Brown, H. Eskes, A. R. Gomes, A. C. Lange, B. C. McDonald, J. Peischl, A. Petzold, C. R. Thompson, A. Kiendler-Scharr; The global impacts of COVID-19 lockdowns on urban air pollution: A critical review and recommendations. Elementa: Science of the Anthropocene, 9 (1): 00176. doi: https://doi.org/10.1525/elementa.2021.00176, 2021.

Granier, C., Darras, S., van der Gon, H.D., Doubalova, J., Elguindi, N., Galle, B., Gauss, M., Guevara, M., Jalkanen, J.P.,
610   Kuenen, J., Liousse, C., Quack, B., Simpson, D., Sindelarova, K. The Copernicus atmosphere monitoring service global and regional emissions (April 2019 version). Copernicus https://doi.org/10.24380/d0bnkx16, 2019.

Guenther, A., Karl, T., Harley, P., Wiedinmyer, C., Palmer, P., Geron, C. Estimates of global terrestrial isoprene emissions using MEGAN (model of emissions of gases and aerosols from nature). Atmos. Chem. Phys. 6, 3181–3210, 2006.

Honoré, C., Rouïl, L., Vautard, R., Beekmann, M., Bessagnet, B., Dufour, A., Elichegaray, C., Flaud, J., Malherbe, L., Meleux,
615   F., Menut, L., Martin, D., Peuch, A., Peuch, V., Poisson, N. Predictability of European air quality: the assessment of three years of operational forecasts and analyses by the PREV'AIR system. J. Geophys. Res. 113, D04301. https://doi.org/10.1029/2007JD008761, 2008.

Janssens-Maenhout, G., Crippa, M., Guizzardi, D., Dentener, F., Muntean, M., Pouliot, T. Keating, Q. Zhang, J. Kurokawa, R. Wankmüller, H. Denier van der Gon, J. J. P. Kuenen, Z. Klimont, G. Frost, S. Darras, B. Koffi, and M. Li. HTAP_v2. 2: a
620   mosaic of regional and global emission grid maps for 2008 and 2010 to study hemispheric transport of air pollution. Atmos. Chem. Phys., 15(19), 11411-11432, 2015.

Kalnay, E., Kanamitsu, M., Kistler, R., Collins, W., Deaven, D., Gandin, L., Iredell, M., Saha, S., White, G., Woollen, J., Zhu, Y., Chelliah, M., Ebisuzaki, W., Higgins, W., Janowiak, J., Mo, K., Ropelewski, C., Wang, J., Leetmaa, A., Reynolds, R., Jenne, R., Joseph, D. The NCEP/NCAR 40-year reanalysis project. Bull. Am. Meteorol. Soc., 437–471 https://
625   doi.org/10.1175/1520-0477(1996)077, 1996.

Le, T., Y. Wang, L. Liu, J. Yang, Y. L. Yung, G. Li, J. H. Seinfeld, Unexpected air pollution with marked emission reductions during the COVID-19 outbreak in China, Science, 369(6504), 702-706, 10.1126/science.abb7431, 2020.

Mailler, S., L. Menut, D. Khvorostiyanov, M. Valari, F. Couvidat, G. Siour, S. Turquey, R. Briant, P. Tuccela, B. Bessagnet, A. Colette, and F. Meleux: CHIMERE-2017: from urban to hemispheric chemistry-transport modeling, Geosci. Model Dev.,
630   10, 2397-2423, 2017.

Mareckova, K., Pinterits, M., Ullrich, B., Wankmueller, R., Gaisbauer, S. EMEP Inventory Review 2019 Review of Emission Data Reported under the LRTAP Convention and NEC Directive. European Environment Agency and CEIP, p. 54, 2019.

Malguzzi, P., Buzzi, A., Drofa, O. The meteorological global model GLOBO at the ISAC-CNR of Italy assessment of 1.5 yr of experimental use for medium-range weather forecasts. Weather and forecasting, 26(6), 1045-1055, 2011.

635   Marécal, V., Peuch, V.H., Andersson, C., Andersson, S., Arteta, J., Beekmann, M., Benedictow, A., Bergström, R., Bessagnet, B., Cansado, A., Chéroux, F., Colette, A., Coman, A., Curier, R.L., Denier van der Gon, H.A.C., Drouin, A., Elbern, H., Emili, E., Engelen, R.J., Eskes, H.J., Foret, G., Friese, E., Gauss, M., Giannaros, C., Guth, J., Joly, M., Jaumouillé, E., Josse, B., Kadygrov, N., Kaiser, J.W., Krajsek, K., Kuenen, J., Kumar, U., Liora, N., Lopez, E., Malherbe, L., Martinez, I., Melas, D., Meleux, F., Menut, L., Moinat, P., Morales, T., Parmentier, J., Piacentini, A., Plu, M., Poupkou, A., Queguiner, S., Robertson,

640   L., Rouïl, L., Schaap, M., Segers, A., Sofiev, M., Tarasson, L., Thomas, M., Timmermans, R., Valdebenito, A., van Velthoven, P., van Versendaal, R., Vira, J., Ung, A. A regional air quality forecasting system over Europe: the MACC-II daily en- semble production. Geosci. Model Dev. 8, 2777–2813. doi:https://doi.org/10.5194/ gmd-8-2777-2015, 2015.

Menut, L., Vautard, R., Flamant, C., Abonnel, C., Beekmann, M., Chazette, P., Flamant, P., Gombert, D., Guédalia, D., Lefebvre, M., Lossec .D.,.M., B., Mégie, G., Perros, P., Sicard, M., Toupance, G. Measurements and modelling of atmospheric

645   pollution over the Paris area: an overview of the ESQUIF project. Ann. Geophys. 18, 1467–1481, 2000.

Menut, L., Coll, I., Cautenet, S. Impact of meteorological data resolution on the forecasted ozone concentrations during the ESCOMPTE IOP 2a and 2b. Atmos. Res. 74, 139–159, 2005a.

Menut, L., Schmechtig, C., Marticorena, B. Sensitivity of the sandblasting fluxes calculations to the soil size distribution accuracy. J. Atmos. Ocean. Technol. 22, 1875–1884, 2005b.

650   Menut, L. and Bessagnet, B. Atmospheric composition forecasting in Europe. Ann. Geophys. 28, 61–74, 2010.

Menut L, B. Bessagnet, D. Khvorostyanov, M. Beekmann, A. Colette, I. Coll, G. Curci, G. Foret, A. Hodzic, S. Mailler, F. Meleux, J.L. Monge, I. Pison, G. Siour, S. Turquety, M. Valari, R. Vautard and M.G. Vivanco: CHIMERE: a model for regional atmospheric composition modelling, Geoscientific Model Development, 6, 981-1028, 2013.

Menut, L., Mailler, S., Siour, G., Bessagnet, B., Turquety, S., Rea, G., Briant, R., Mallet, M., Sciare, J., Formenti, P., Meleux,

655   F. Ozone and aerosol tropospheric concentrations variability analyzed using the ADRIMED measurements and the WRF and CHIMERE models. Atmos. Chem. Phys. 15, 6159–6182. https://doi.org/10.5194/acp- 15-6159-2015, 2015a.

Menut, L., Rea, G., Mailler, S., Khvorostyanov, D., Turquety, S. Aerosol forecast over the Mediterranean area during July 2013 (ADRIMED/CHARMEX). Atmos. Chem. Phys. 15, 7897–7911. https://doi.org/10.5194/acp-15-7897-2015, 2015b.

Menut, L., B. Bessagnet, G. Siour, S. Mailler, R. Pennel, A. Cholakian, Impact of lockdown measures to combat Covid-19 on

660   air quality over western Europe, Scie. Total Env., 741, 140426, https://doi.org/10.1016/j.scitotenv.2020.140426, 2020.

Mertens, M., Jöckel, P., Matthes, S., Nützel, M., Grewe, V., Sausen, R.. COVID-19 induced lower-tropospheric ozone changes. Env. Res. Lett., 16(6), 064005, 2021.

Monahan, E.C. In the Role of Air-Sea Exchange in Geochemical Cycling. Kluwer Academic Publishers, Dordrecht, Holland, pp. 129–163 chapter "The ocean as a source of atmospheric particles", 1986.

665   Muhammad, S., Long, X., Salman, M. COVID-19 pandemic and environmental pollution: A blessing in disguise? Scie. Total Env., 728, 138820, 2020.

Ordóñez, C., J. M. Garrido-Perez, R. García-Herrera, Early spring near-surface ozone in Europe during the COVID-19 shutdown: Meteorological effects outweigh emission changes, Science of The Total Environment, 747, 141322, ISSN 0048-9697, https://doi.org/10.1016/j.scitotenv.2020.141322, 2020.

670 Pazmiño, A., Beekmann, M., Goutail, F., Ionov, D., Bazureau, A., Nunes-Pinharanda, M., Hauchecorne, A., and Godin-Beekmann, S.: Impact of COVID-19 pandemic related to lockdown measures on tropospheric NO2 columns over Île-de-France, Atmos. Chem. Phys. Discuss., https://doi.org/10.5194/acp-2021-456, in review, 2021.

Rouïl, L., Honoré, C., Vautard, R., Beekmann, M., Bessagnet, B., Malherbe, L., Meleux, F., Dufour, A., Elichegaray, C., Flaud, J., Menut, L., Martin, D., Peuch, A., Peuch, V., Poisson, N. PREV'AIR: an operational forecasting and mapping system

675 for air quality in Europe. BAMS 90, 73–83. https://doi.org/10.1175/2008BAMS2390.1, 2009.

Skamarock, W., Klemp, J., Dudhia, J., Gill, D., Barker, D., Wang, W., Powers, J. A description of the advanced research wrf version 2. NCAR Technical Note, Boulder, Colorado, USA, NCAR/TN–468+STR, 2007.

Shi, X. and Brasseur, G.P. The response in air quality to the reduction of Chinese economic activities during the COVID-19 outbreak. Geophys. Res. Lett., 47(11), e2020GL088070. https://doi.org/10.1029/2020GL088070, 2020.

680 Sicard, P., De Marco, A., Agathokleous, E., Feng, Z., Xu, X., Paoletti, E., J. J. Diéguez Rodriguez, Calatayud, V. Amplified ozone pollution in cities during the COVID-19 lockdown. Scie. Total Env., 735, 139542, 2020.

Souri, A. H., K. Chance, J. Bak, C.R. Nowlan, G. González Abad, Y. Jung, D. C. Wong, J. Mao, X. Liu. Unraveling Pathways of Elevated Ozone Induced by the 2020 Lockdown in Europe by an Observationally Constrained Regional Model: Non-Linear Joint Inversion of NO x and VOC Emissions using TROPOMI. Atmos. Chem. Phys. Dis., 1-45. 2021.

685 Steinbrecht, W., Kubistin, D., Plass-Dülmer, C., Davies, J., Tarasick, D. W., Gathen, P. V. D., ... Cooper, O. R. COVID-19 crisis reduces free tropospheric ozone across the Northern Hemisphere. Geophys. Res. Lett., 48(5), e2020GL091987, 2021.

Szopa S., G.Foret, L.Menut, A.Cozic, 2009, Impact of large scale circulation on European summer surface ozone: consequences for modeling, Atmospheric Environment, 43(6), 1189-1195, doi:10.1016/j.atmosenv.2008.10.039, 2009.

Thunis, P., Clappier, A., Beekmann, M., Putaud, J., Cuvelier, C., Madrazo, J., de Meij, A. Non-linear response of PM2.5 to

690 changes in NOx and NH3 emissions in the Po basin (Italy): consequences for air quality plans. Atmos. Chem. Phys., 21, 9309–9327, 10.5194/acp-2021-65, 2021.

Vautard, R., Beekmann, M., Menut, L. Applications of adjoint modelling in atmospheric chemistry: sensitivity and inverse modelling. Environ. Model. Softw. 15, 703–709, 2000.

Vivanco, M., Bessagnet, B., Cuvelier, C., Theobald, M., Tsyro, S., Pirovano, G., Aulinger, A., Bieser, J., Calori, G., Ciarelli,

695 G., Manders, A., Mircea, M., Aksoyoglu, S., Briganti, G., Cappelletti, A., Colette, A., Couvidat, F., D'Isidoro, M., Kranenburg, R., Meleux, F., Menut, L., Pay, M., Rouil, L., Silibello, C., Thunis, P., Ung, A. Joint analysis of de- position fluxes and atmospheric concentrations of inorganic nitrogen and sulphur compounds predicted by six chemistry transport models in the frame of the EURODELTAIII project. Atmos. Environ. 151, 152–175. https://doi.org/10.1016/j. atmosenv.2016.11.042, 2017.

Wilson, R. C., Fleming, Z. L., Monks, P. S., Clain, G., Henne, S., Konovalov, I. B., Szopa, S., Menut, L. Have primary emission
700   reduction measures reduced ozone across Europe? An analysis of European rural background ozone trends 1996–2005.
Atmospheric Chemistry and Physics, 12(1), 437-454, 2012.

705 **Table 1.** Brief description of the two setups of the CHIMERE model, used for the simulations of ozone distribution over Europe in April 2019 and April 2020 (STD and COVID scenario).

	CHIMERE C1	**CHIMERE C2**
Horizontal resolution	20×20 km^2	20×20 km^2
Vertical resolution	15 levels from 998 to 300 hPa	15 levels from 998 to 300 hPa
Biogenic emissions	MEGAN online model	MEGAN online model
Inventory of anthropogenic emissions for STD simulations	HTAP v2.2 for 2010, monthly	EMEP for 2017, seasonal modulation
Modifications of anthropogenic emissions for the COVID scenario	Based on the change of emissions in the 5 most populated European countries in the COVID inventory from CAMS	Based on the decrease in traffic according to the "driving" database from Apple, discriminated by country
Meteorological fields	BOLAM meteorological model	WRF meteorological model
Boundary conditions for meteorology	GLOBO global model initialized daily by NCEP/GFS global fields	NCEP/GFS global fields
Boundary conditions for trace gas concentrations	Climatology from the LMDz-INCA model	CHIMERE simulations over a larger domain englobing northern Africa and using anthropogenic emissions from CAMS

710 **Table 2.** Changes of surface ozone concentrations between 1-15 April 2020 and the same period in 2019, for 4 target regions in Europe (rectangles in Fig. 3a), derived from surface in situ measurements. Total, meteorological and lockdown-associated changes are considered in mixing ratio units (ppb), for daily averages and maximum daily 8-hour running averages (also percentage in italics). Values after ± indicate one standard deviation.

Surface $\Delta O_3^{2020\text{-}2019}$ in 1-15 April				
	Central Europe 43-52°N 0-20°E	**Benelux to Northern Italy band** 44-52°N 4-10°E	**North-eastern Europe** 51-54°N 12-23°E	**South-western Europe** 37-45°N 9°W-0°
Total change for daily averages	3.5 ± 5.5 ppb	4.8 ± 4.8 ppb	-3.2 ± 3.5 ppb	-4.0 ± 6.1 ppb
Lockdown effect for daily averages	0.1 ± 6.7 ppb	1.2 ± 6.2 ppb	-3.5 ± 4.4 ppb	-3.3 ± 6.1 ppb
Total change for MDA8	10.0 ± 6.3 ppb *26.2 ± 31.0 %*	12.1 ± 5.4 ppb *30.0 ± 15.0 %*	0.1 ± 3.7 ppb *0.6 ± 8.5 %*	-5.4 ± 5.8 ppb *-10.4 ± 15.5 %*
Meteorological effect for MDA8	8.1 ± 3.2 ppb *19.6 ± 11.8 %*	9.2 ± 3.3 ppb *21.9 ± 8.8 %*	3.2 ± 1.0 ppb *6.7 ± 2.4 %*	0.0 ± 7.2 ppb *1.4 ± 4.1 %*
Lockdown effect for MDA8	3.7 ± 5.8 ppb *10.7 ± 26.7 %*	5.1 ± 4.9 ppb *13.1 ± 12.5 %*	-2.0 ± 3.7 ppb *-4.0 ± 8.4 %*	-4.5 ± 6.1 ppb *-7.9 ± 17.1 %*

715

Table 3. Same as Table 2 but for the whole month of April

Surface $\Delta O_3^{2020-2019}$ in 1-30 April				
	Central Europe 43-52°N 0-20°E	**Benelux to Northern Italy band** 44-52°N 4-10°E	**North-eastern Europe** 51-54°N 12-23°E	**South-western Europe** 37-45°N 9°W-0°
Total change for daily averages	1.3 ± 4.9 ppb	1.95 ± 4.6 ppb	-2.7 ± 3.1 ppb	-4.2 ± 5.1 ppb
Lockdown effect for daily averages	-0.5 ± 5.2 ppb	0.3 ± 4.3 ppb	-3.9 ± 3.5 ppb	-2.8 ± 5.1 ppb
Total change for MDA8	4.6 ± 5.2 ppb *11.0 ± 13.6 %*	5.4 ± 4.4 ppb *12.3 ± 9.9 %*	-1.5 ± 3.7 ppb *-2.7 ± 8.0 %*	-6.1 ± 5.9 ppb *-11.6 ± 15.0 %*
Meteorological effect for MDA8	5.1 ± 2.3 ppb *11.7 ± 6.2 %*	5.4 ± 2.7 ppb *11.8 ± 6.1 %*	3.1 ± 0.9 ppb *6.3 ± 2.1 %*	-0.5 ± 1.9 ppb *-2.3 ± 3.5 %*
Lockdown effect for MDA8	0.3 ± 4.8 ppb *1.4 ± 11.9 %*	1.1 ± 4.0 ppb *2.9 ± 8.7 %*	-3.9 ± 3.8 ppb *-7.7 ± 8.3 %*	-4.5 ± 6.0 ppb *-8.0 ± 15.9 %*

Table 4. Statistics of the comparisons of in situ surface observations with respect to IASI+GOME2 lowermost tropospheric
720 ozone retrievals and model simulations.

	Surface meas. (daily average) vs. IASI+GOME2 1-15 April	Surface meas. (8-10 UTC morning) vs. IASI+GOME2 1-15 April	Surface meas. (daily average) vs. IASI+GOME2 1-30 April	Surface meas. (daily average) CHIMERE C1 1-15 April	Surface meas. (daily average) CHIMERE C2 1-15 April
Bias (ppb)	-8.6	-10.2	-7.1	0.9	1.4
Correlation R	0.55	0.54	0.46	0.58	0.44
RMS difference (ppb)	11.8	13.3	10.0	7.3	7.7
Ratio of standard deviations $\sigma y / \sigma x$	1.03	0.93	0.97	0.41	0.36

725   **Table 5.** Comparison of nitrogen dioxide concentrations in the period 1-15 April 2019 and the changes between this period in 2020 with respect to 2019, for 2 target regions in Europe (rectangles in Fig. 3a), derived from surface in situ measurements and model simulations with the configurations C1 and C2. Surface concentrations and vertically integrated total columns are compared. Values after ± indicate one standard deviation. For lack of representativity, model standard deviation within the Paris sector is not given.

	Benelux to Northern Italy band 44-52°N 4-10°E			Paris 48.6-49.0°N 2.3-2.8°E		
	In situ meas.	CHIMERE C1	CHIMERE C2	In situ meas.	CHIMERE C1	CHIMERE C2
Surface NO_2^{2019}	8.9 ± 4.3 ppb	6.8 ± 4.7 ppb	2.5 ± 2.0 ppb	18.3 ± 2.6 ppb	15.0 ppb	8.9 ppb
Surface $\Delta NO_2^{2020\text{-}2019}$	1.2 ± 3.1 ppb -14 ± 35 %	3.7 ± 0.6 ppb -54 ± 9 %	0.8 ± 0.5 ppb -32 ± 20 %	7.0 ± 1.8 ppb -38 ± 10 %	6.5 ppb -43 %	1.3 ppb -15 %
NO_2^{2019} total column		4.4 ± 3.3 10^{15} mol cm^{-2}	3.2 ± 2.4 10^{15} mol cm^{-2}		$9.6 \ 10^{15}$ mol cm^{-2}	$7.4 \ 10^{15}$ mol cm^{-2}
$\Delta NO_2^{2020\text{-}2019}$ total column		2.5 ± 0.5 10^{15} mol cm^{-2} -56 ± 11 %	0.7 ± 1.0 10^{15} mol cm^{-2} -21 ± 30 %		$6.0 \ 10^{15}$ mol cm^{-2} 63 %	$0.4 \ 10^{15}$ mol cm^{-2} -5 %

730
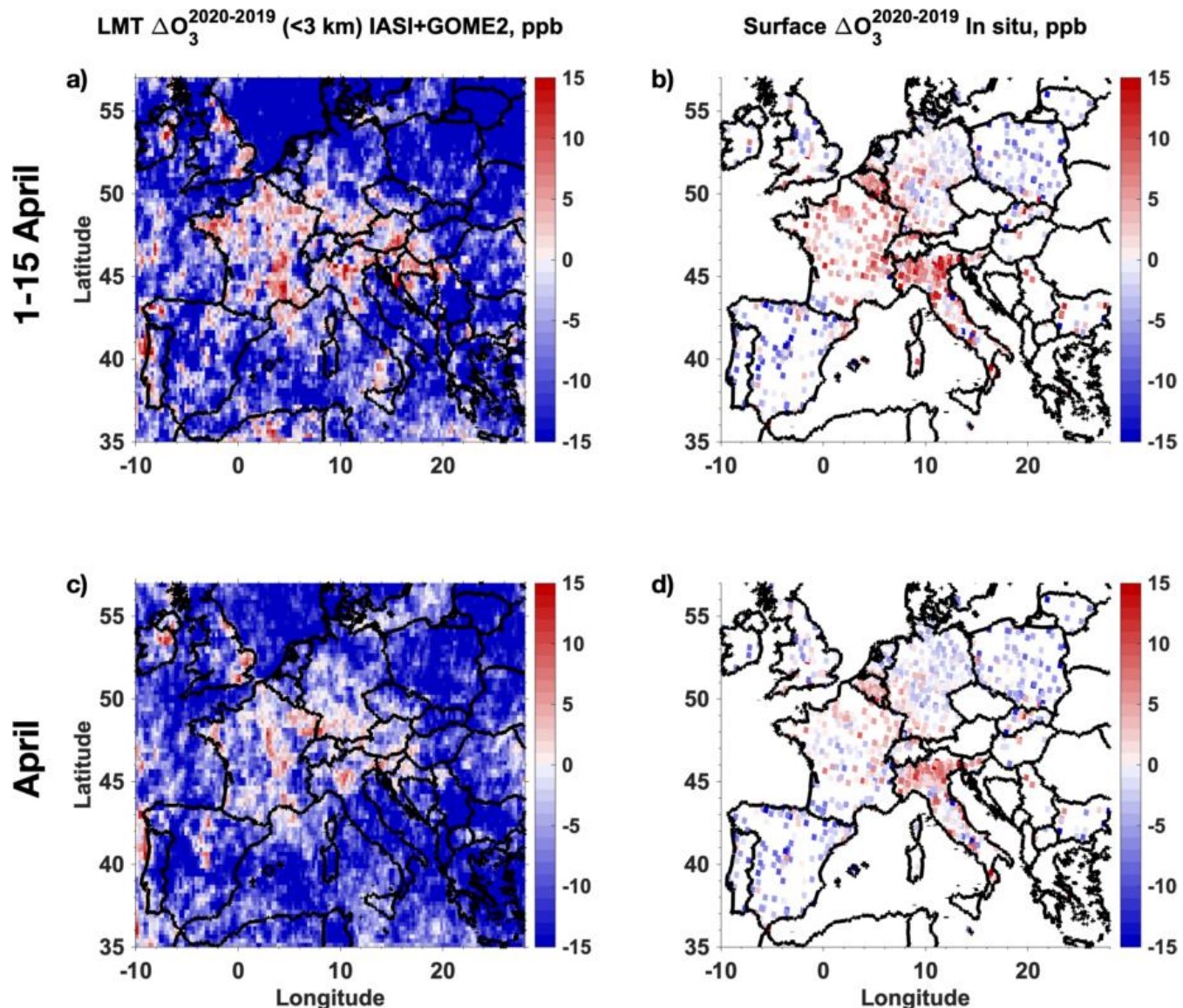
Figure 1. Changes $\Delta O_3^{2020-2019}$ in ozone concentrations (ppb) between the average on 1-15 April 2020 and that of the same period in 2019 observed **(a)** at the lowermost troposphere (below 3 km of altitude) by the IASI+GOME2 multispectral satellite approach and **(b)** at the surface by in situ sensors from the EEA network. **(c, d)** Same as (a, b) but for the whole month of April. We consider here only surface in situ data coincident in time and space with the satellite retrievals (on daily basis). Therefore, the temporal and spatial sampling of both datasets is the same.

740
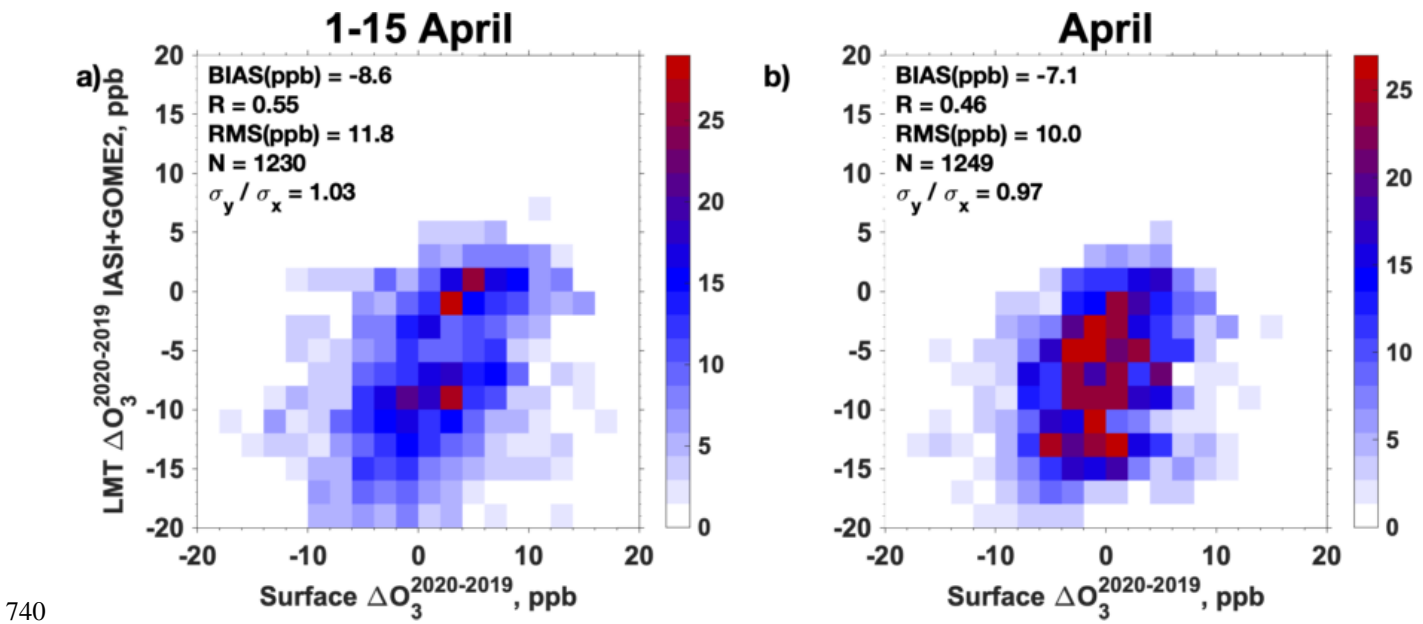
Figure 2. Scatterplot **(a)** IASI+GOME2 retrievals with respect to colocalized surface in situ measurement of $\Delta O_3^{2020\text{-}2019}$ differences in ozone concentrations averaged over 1-15 April 2020 with respect to averages in the same period in 2019. The colorscale represents the number of occurrences of points within each sector of 2×2 ppb. **(b)** Same as (a) but for the whole month of April.

745
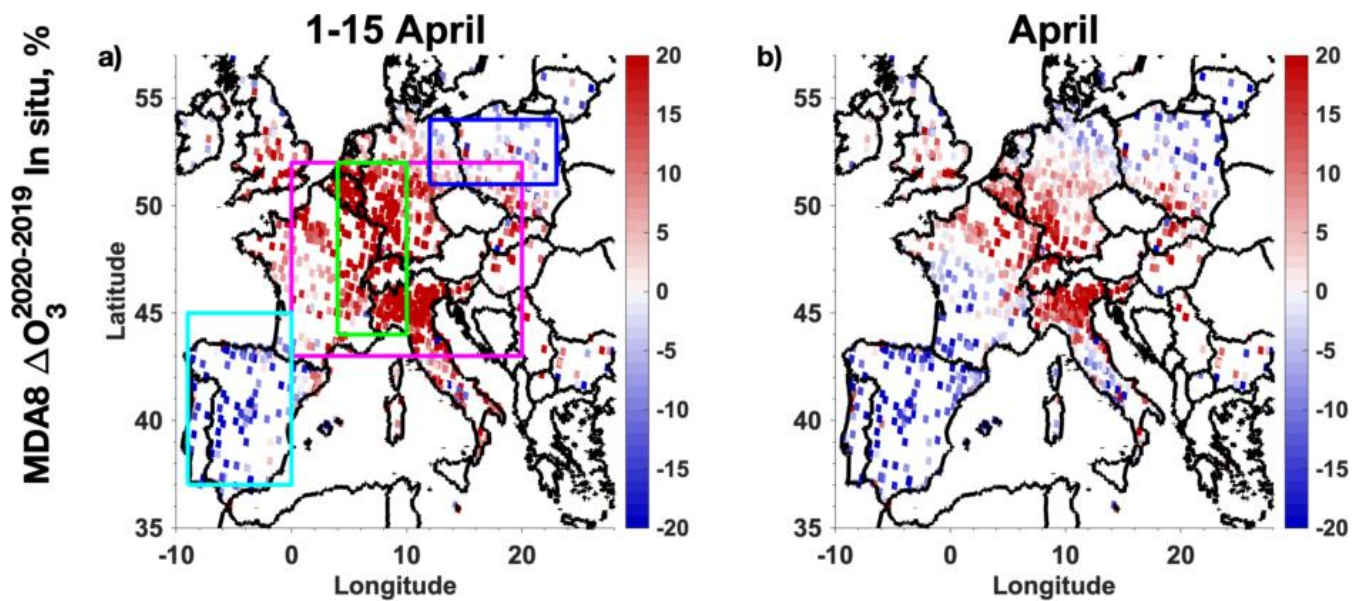
Figure 3. Relative changes (in %) in maximum daily average during 8h (MDA8) of surface ozone concentrations measured by in situ sensors between 2020 and 2019, during the periods **(a)** 1-15 April and **(b)** 1-30 April. Percentages are calculated with respect to averages in 2019 for the corresponding period. Rectangles in panel (a) indicate the target regions indicated in

750   the text and Tables 2 to 5.
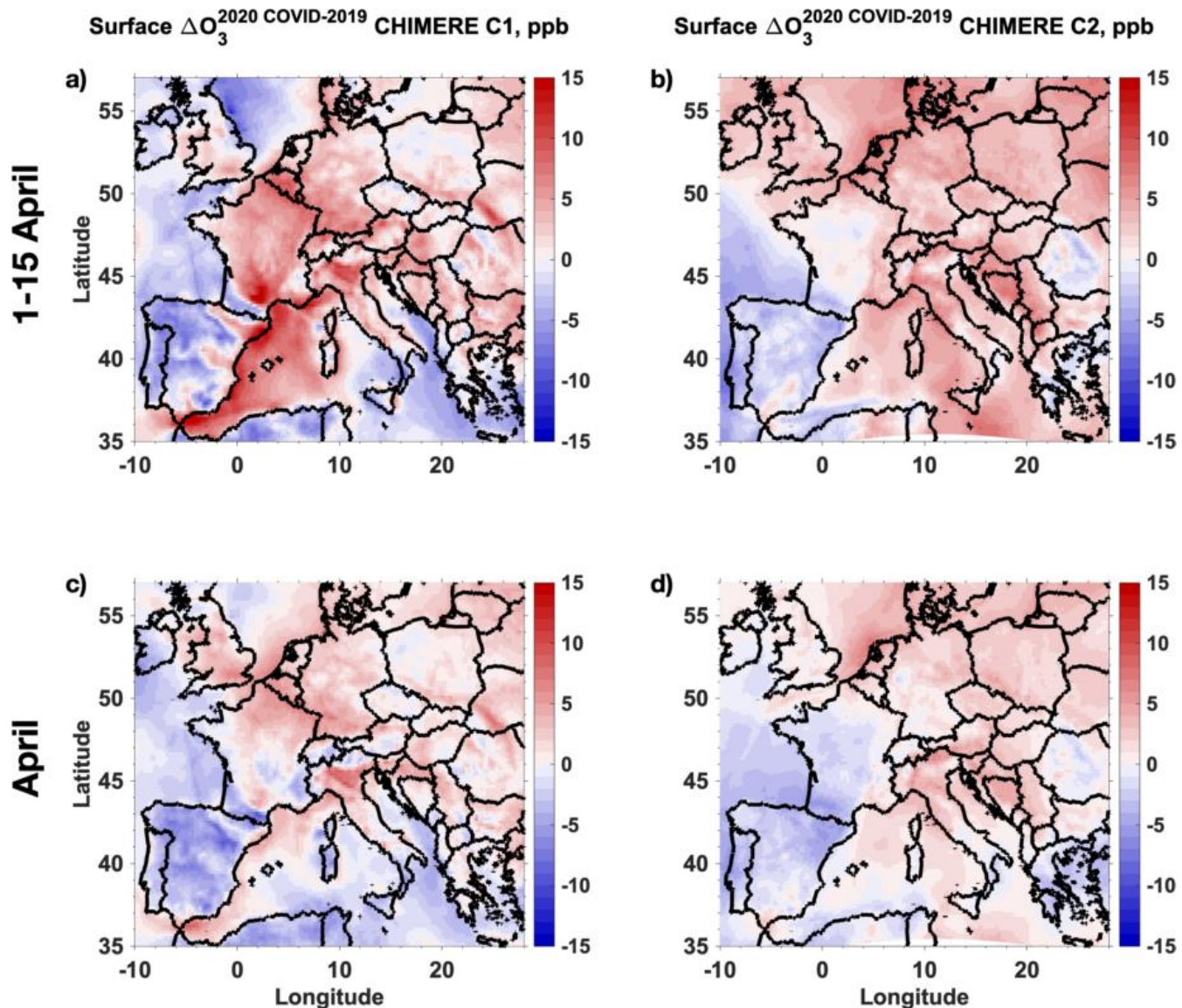
Figure 4. Idem as Figure 1 but for simulated $\Delta O_3^{2020-2019}$ with the CHIMERE model with the configuration **(a, c)** C1 and **(b, d)** C2. Panels (a, b) consider the period 1-15 April and (c, d) the whole month of April.

755
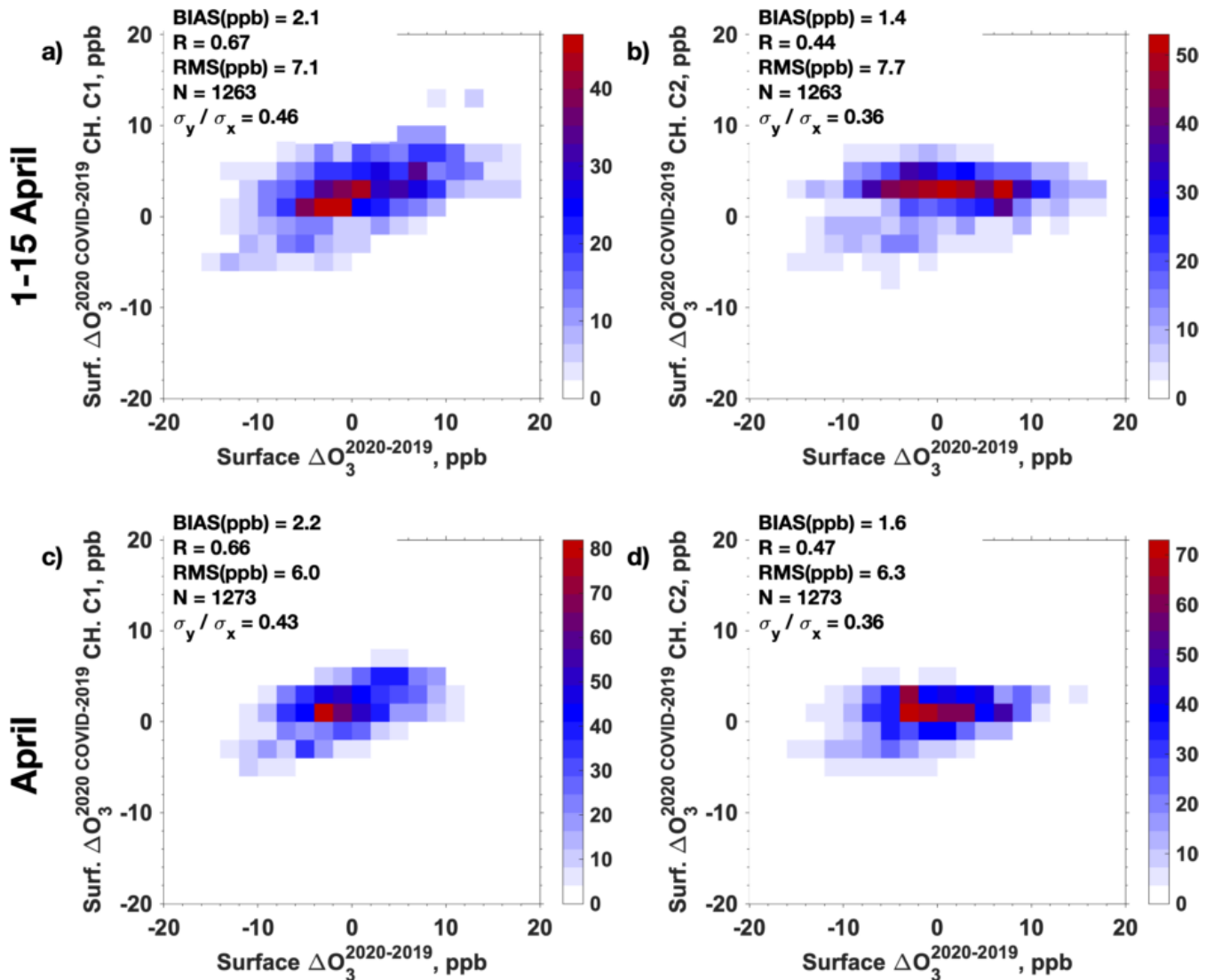
Figure 5. Idem as Figure 2 but for simulated $\Delta O_3^{2020\text{-}2019}$ with the CHIMERE model with the configuration (a) C1 and (b) C2.

760
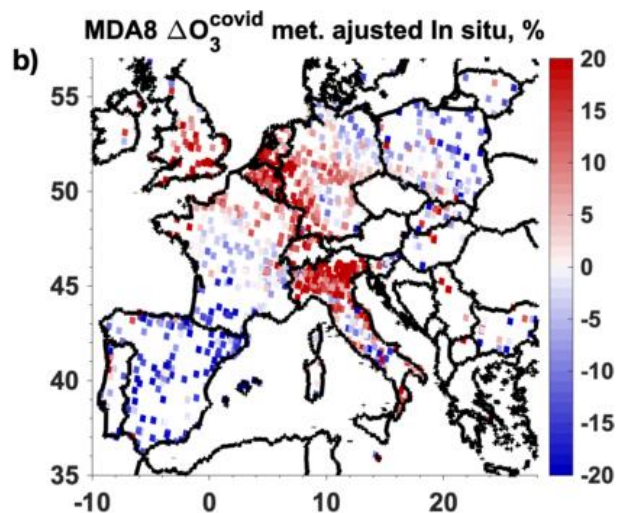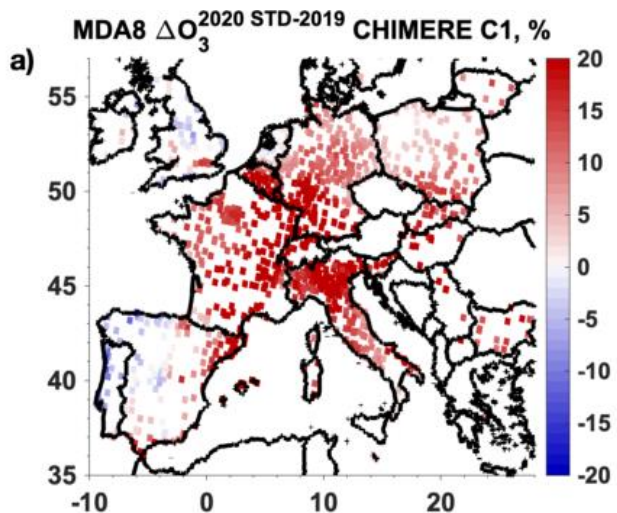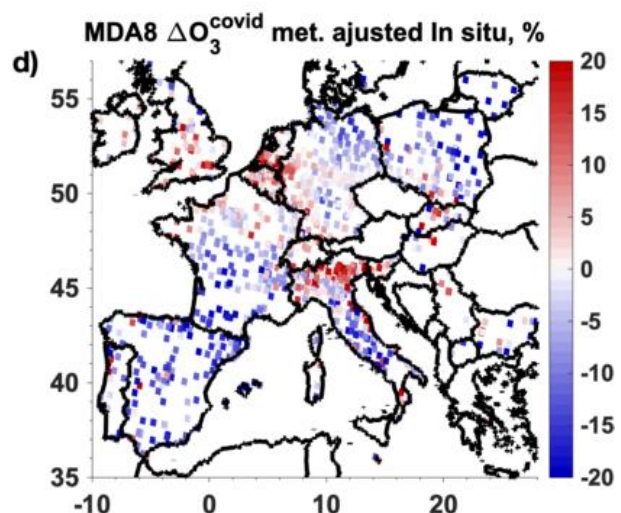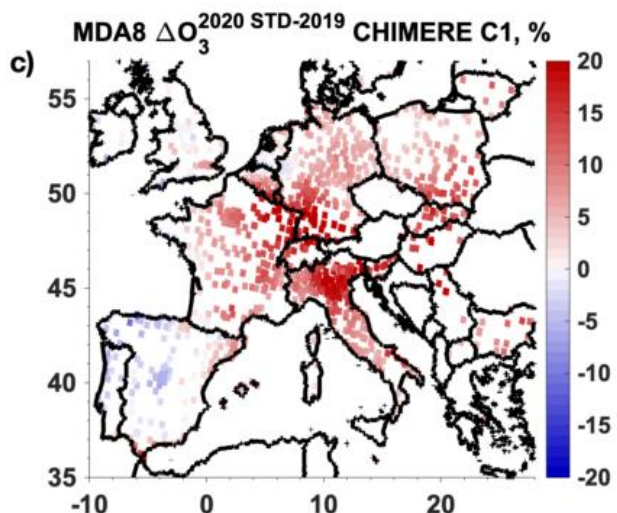
Figure 6. Relative changes (in %) in maximum daily average during 8h (MDA8) of surface ozone concentrations **(a)** associated with meteorological conditions derived from the difference between CHIMERE C1 simulations in 2020 using STD emissions and 2019 and **(b)** related with the pandemic lockdown in 2020 measured by in situ sensors and adjusted for withdrawing the effects of meteorological conditions using equation 1, averaged over the period of 1-15 April. **(c)** Idem of (a) and **(d)** idem of (b) but averaged over the whole month of April.
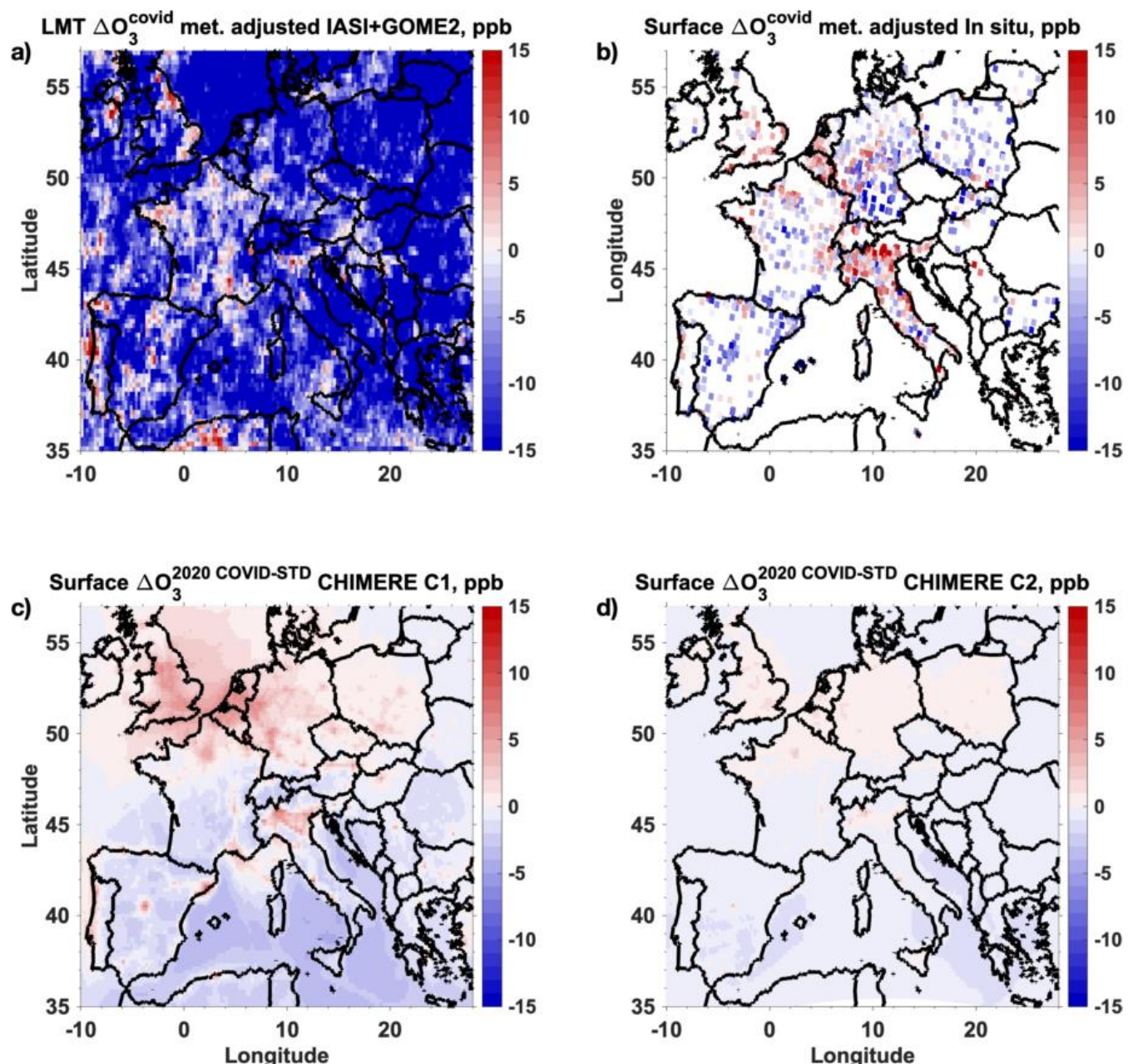
770 **Figure 7.** Changes in ozone pollution (ppb) associated with the pandemic lockdown in 1-15 April 2020, derived from adjusted observations (using Eq. 1) for avoiding the influence of meteorological conditions at **(a)** the lowermost troposphere (LMT, < 3 km asl) retrieved with IASI+GOME2 multispectral satellite approach and the surface **(b)** measured by in situ sensors and simulated by the CHIMERE model with the **(c)** C1 and **(d)** C2 setups.
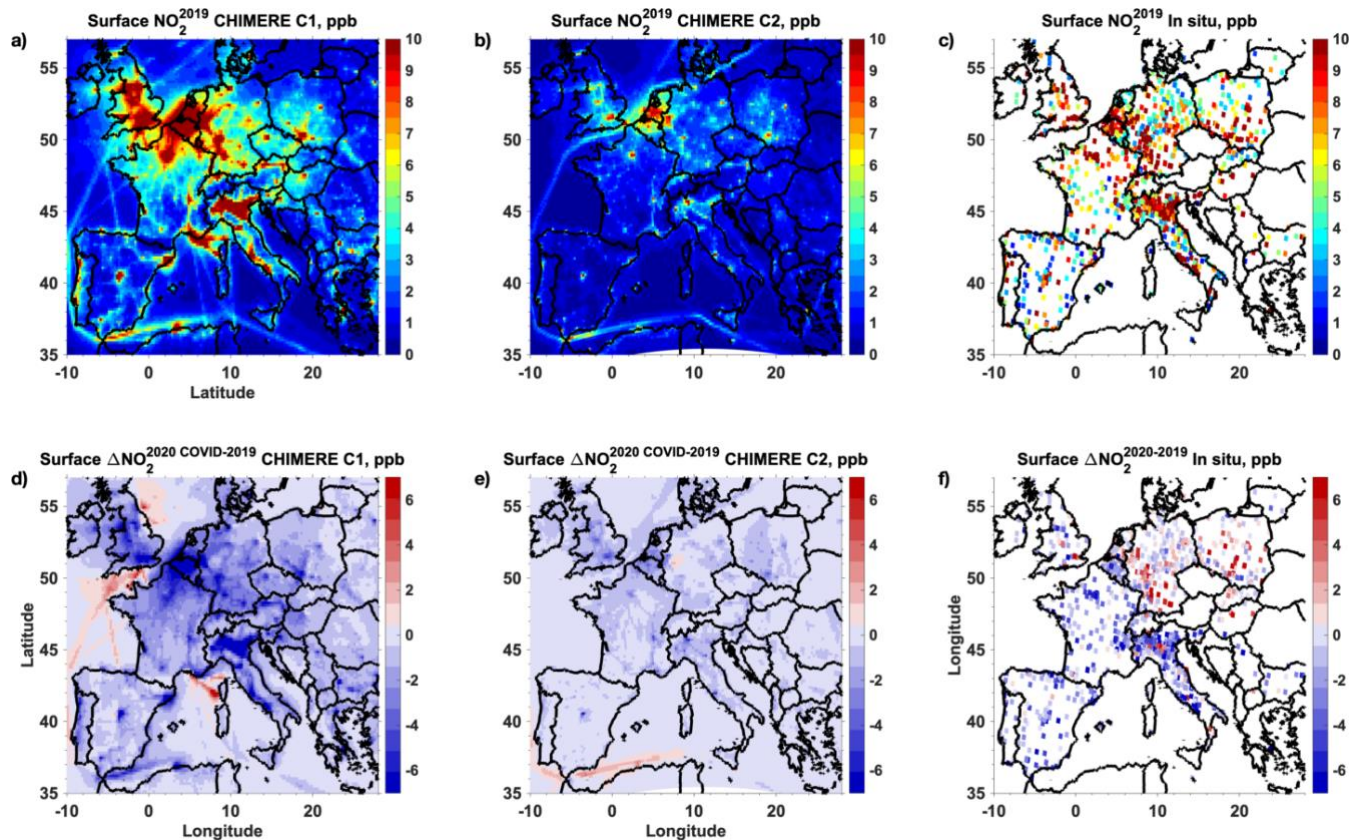
Figure 8. Surface NO$_2$ concentrations (ppb) averaged over the period 1-15 April 2019 simulated by the CHIMERE with the configurations **(a)** C1 and **(b)** C2, as well as **(c)** measured by in situ sensors. **(d)** Idem of (a), **(e)** of (b) and **(f)** of (c) but for changes between 1-15 April 2020 with respect to the same period in 2019.

775
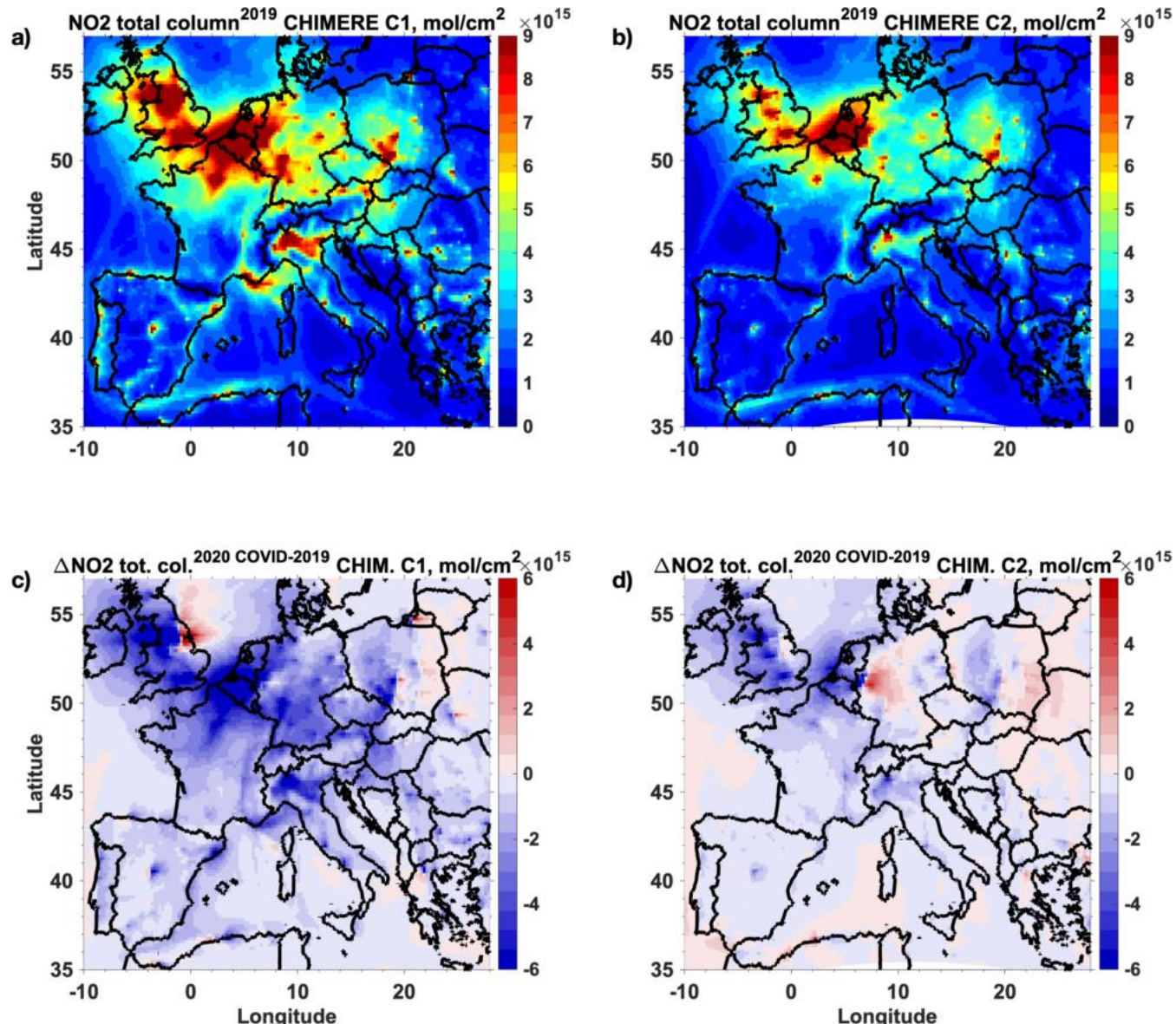
Figure 9. Total columns of NO_2 (molecules cm^{-2}) averaged over the period 1-15 April 2019 simulated by the CHIMERE with the configurations **(a)** C1 and **(b)** C2. **(c)** Idem of (a) and **(d)** of (b) but for changes between 1-15 April 2020 with respect to the same period in 2019.
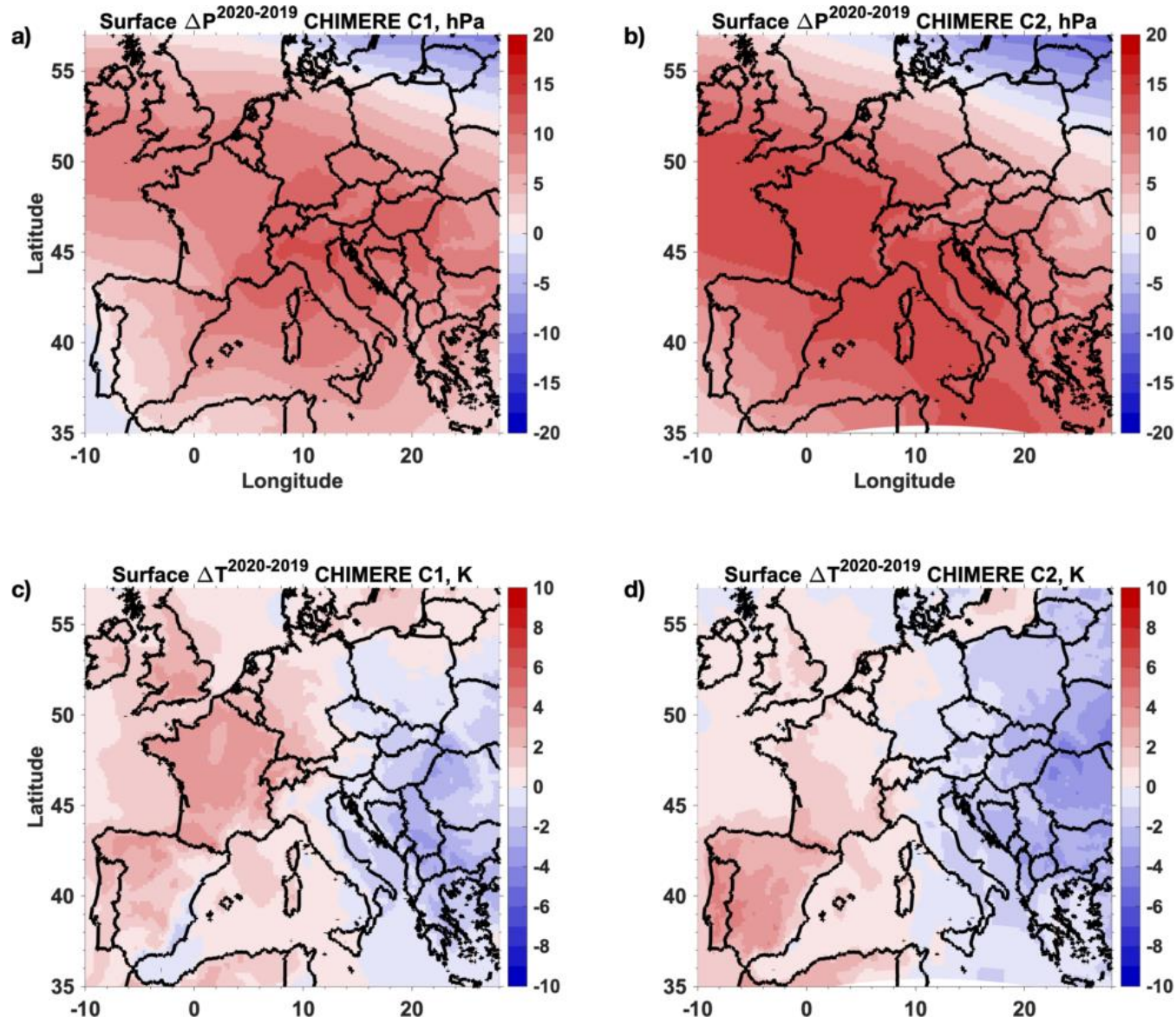
Figure 10. Changes in **(a)** surface pressure (hPa) and **(c)** surface temperature (K) averaged over the period 1-15 April 2020 with respect to the same period in 2019 from the meteorological fields used by CHIMERE with the configuration C1. **(b)** Idem of (a) and **(d)** idem of (c) but for CHIMERE with the configuration C2.

790